J. Physiol. (1986), **377**, *pp.* 89–141
With 17 *text-figures*
Printed in Great Britain

PROPERTIES OF THE METALLOCHROMIC DYES ARSENAZO III, ANTIPYRYLAZO III AND AZO1 IN FROG SKELETAL MUSCLE FIBRES AT REST

BY S. M. BAYLOR, S. HOLLINGWORTH, C. S. HUI* AND M. E. QUINTA-FERREIRA†

*From the ‡ Department of Physiology, University of Pennsylvania, Philadelphia, PA 19104, U.S.A., and the * Departments of Physiology/Biophysics and Medicine, Indiana University, Indianapolis, IN 46223, U.S.A.*

(*Received 31 July 1985*)

SUMMARY

1. Intact single twitch fibres from frog muscle were isolated and mounted in a normal Ringer solution (16 °C) on an optical bench apparatus for measuring fibre absorbance as a function of the wave-length and polarization of the incident light. Fibre absorbance was measured in resting fibres both in the absence and in the presence of one of three metallochromic dyes: Arsenazo III, Antipyrylazo III and Azo1.

2. In the absence of dye, the fibre intrinsic absorbance, $A_i(\lambda)$, measured as a function of wave-length, λ, was well described by the equation:

$$A_i(\lambda) = A_i(\lambda_{long})\,(\lambda_{long}/\lambda)^X,$$

where λ_{long} is a reference wave-length selected to lie beyond the absorbance band of the dyes and X is the exponential index. For wave-lengths between 480 and 810 nm, the average value of X was 1·1 for 0 deg polarized light (electric vector parallel to the fibre axis) and 1·3 for 90 deg polarized light (electric vector perpendicular to the fibre axis). The intrinsic absorbance at 0 deg, $A_{i,0}(\lambda)$, was somewhat larger than the intrinsic absorbance at 90 deg, $A_{i,90}(\lambda)$; for example, on average ($n = 6$), $A_{i,0}$ (810 nm) was 0·22, whereas $A_{i,90}$ (810 nm) was 0·016.

3. Following dye injection, dye-related absorbance was estimated from the measured total fibre absorbance by subtracting the component attributable to the intrinsic absorbance; additionally, for comparison with *in vitro* calibrations as a function of wave-length, myoplasmic dye absorbance was corrected for the steady change in dye concentration with time that was attributable to dye diffusion.

4. In fibres injected with either Arsenazo III or Antipyrylazo III, the dye-related absorbance measured with 0 deg light, $A_0(\lambda)$, was found to be significantly greater than that measured with 90 deg light, $A_{90}(\lambda)$, indicating the presence of a resting 'dichroic' signal, $A_0(\lambda) - A_{90}(\lambda)$, attributable to bound and oriented dye molecules.

† Current address: Departamento de Fisica, Universidade de Coimbra, 3000 Coimbra, Portugal.
‡ Address for correspondence.

On average, the lower limit estimated for the percentage of oriented dye was 2·8–3·0 % for Antipyrylazo III and 1·5–1·8 % for Arsenazo III, the population differences between the two dyes being statistically significant. The actual percentage of bound and oriented dye molecules is likely to be considerably larger for both dyes.

5. For Arsenazo III, the wave-length dependence of the dichroic signal was not distinguishably different from the 'isotropic' signal, defined as $(A_0(\lambda)+2A_{90}(\lambda))/3$, which represents the average spectrum of all the dye molecules independent of orientation. On the other hand, for Antipyrylazo III the dichroic spectrum appeared to be shifted significantly towards longer wave-lengths ('red-shifted') compared with the isotropic spectrum. From the magnitudes of the isotropic and dichroic absorbances at 650 nm compared with those measured in cuvette calibrations, it was estimated that roughly one-third of the Antipyrylazo III molecules in myoplasm might be bound.

6. When 'best-fitted' by cuvette calibrations measured as a function of free Mg^{2+} concentration, $[Mg^{2+}]$, the Arsenazo III isotropic spectra (520 nm $\leqslant \lambda \leqslant$ 700 nm), on average, indicated a myoplasmic free $[Mg^{2+}]$ of 2·3 mM; the Antipyrylazo III spectra (520 nm $\leqslant \lambda \leqslant$ 620 nm), on average, indicated $[Mg^{2+}]$ to be 0·8 mM if the spectra were uncorrected for the effects of bound dye, or 1·7 mM if the spectra were corrected for the red-shifting effects of bound dye (all estimates assuming a myoplasmic pH of 6·9). However, the estimates for $[Mg^{2+}]$ cannot yet be considered reliable because of incomplete characterization of the amounts and properties of bound dye. For example, interference from bound dye presumably accounts for the finding that the $[Mg^{2+}]$ estimates obtained with Arsenazo III varied significantly as a function of wave-length.

7. Myoplasmic absorbance spectra were also determined for Azo1 (Tsien, 1983), a dye which binds Ca^{2+} with a dissociation constant of 3·7 μM (20 °C) but which is quite insensitive to H^+ and Mg^{2+}. No resting dichroic signal was detected from Azo1 at concentrations in the myoplasm $\leqslant$ 0·5 mM. In one well-resolved experiment (at 0·5 mM-dye) the Azo1 isotropic spectrum for wave-lengths greater than 480 nm appeared to be red-shifted compared with any cuvette calibration for Ca^{2+}. However, because of uncertainties about the fraction of Azo1 that is bound in myoplasm as well as difficulties in accurately measuring dye absorbance on the optical bench at wave-lengths less than 480 nm, no useful information was obtained from Azo1 about the resting levels of the concentration of myoplasmic free Ca^{2+}, $[Ca^{2+}]$.

8. In a number of experiments, measurements were made of dye concentration as a function of time after injection and of longitudinal distance from the injection site, so that the dye's apparent diffusion constant, D_{app}, could be estimated. The average values were: for Antipyrylazo III ($n = 8$), $0{\cdot}21 \times 10^{-6}$ cm^2 s^{-1}; for Arsenazo III ($n = 3$), $0{\cdot}12 \times 10^{-6}$ cm^2 s^{-1}; for Azo1 ($n = 4$), $0{\cdot}10 \times 10^{-6}$ cm^2 s^{-1}. These values are four to nine times smaller than estimates extrapolated from the data of Kushmerick & Podolsky (1969) for myoplasmic diffusivities of molecules of molecular weight about 700. One explanation for the unexpectedly small measured values of D_{app} is that three-quarters to eight-ninths of the dyes are bound in the myoplasm to effectively immobile sites.

9. In one experiment with Antipyrylazo III, enough information was available to calculate D_{app} at four different times following dye injection. D_{app} was observed to

decrease significantly with time, a finding not expected if the amount of bound dye is always small or if the amount of bound dye is linearly proportional to the level of free dye.

10. By means of a computer simulation of the process of longitudinal dye diffusion it was found that the time course of the decline in D_{app} observed for Antipyrylazo III could be explained by the assumption of diffusion with saturable binding. Although the concentration of binding sites and the dissociation constant for dye binding could not be uniquely determined from the information available, the results of the simulation indicate that a large fraction of the Antipyrylazo III molecules, perhaps as much as 75–89 % under the usual recording conditions, were not freely diffusible.

11. Over-all, the results strongly suggest that accurate calibrations of $[Mg^{2+}]$ or $[Ca^{2+}]$ in cytoplasm, either at rest or during activity, by means of metallochromic dyes cannot be carried out in a reliable fashion unless the properties of bound dye molecules are taken into account.

12. An Appendix is included which analyses the *in vitro* spectral properties of Antipyrylazo III as a function of dye concentration and of free $[Mg^{2+}]$. The dye chemistry was found to be more complicated than had been indicated by previous reports. The major complications observed in the absence of Ca^{2+} appear to be due to (i) the formation of metal-free dimers (dissociation constant estimated to be 4·0 mM), and (ii) the formation of a second type of Mg^{2+}–dye complex, possibly a 1 Mg^{2+}:2 dye complex, that produces an absorbance increase at 720 nm, the wave-length most commonly used to monitor changes in the Ca^{2+}–dye complex.

INTRODUCTION

Activation of the myofilaments in a skeletal muscle fibre is known to depend on a transient rise in the myoplasmic free calcium concentration, $\Delta[Ca^{2+}]$. In recent years, work in a number of laboratories has shown that the metallochromic indicator dyes Arsenazo III and Antipyrylazo III can be introduced into the myoplasmic space and that dye absorbance signals detected during activity may be used to gain information about the amplitude and time course of $\Delta[Ca^{2+}]$ (Miledi, Parker & Schalow, 1977, 1979; Baylor, Chandler & Marshall, 1979, 1982*a*,*b*,*c*; Kovacs, Rios & Schneider, 1979, 1983; Schneider, Rios & Kovacs, 1981; Palade & Vergara, 1981, 1982; Miledi, Parker & Zhu, 1982, 1983*a*, *b*; Baylor, Quinta-Ferreira & Hui, 1983, 1985; Kovacs & Szucs, 1983; Kovacs, Schumperli & Szucs, 1983; Ochi & Matsumura, 1984; Close & Lannergren, 1984; Irving, Chandler, Maylie & Sizto, 1985; Maylie, Chandler, Irving & Sizto, 1985; Rios, Stefani, Brum & Goldman, 1985). In addition, by means of quantitative modelling (Baylor, Chandler & Marshall, 1983, 1984; Melzer, Rios & Schneider, 1984, 1986; Quinta-Ferreira, Baylor & Hui, 1984*b*) the dye signals have been used to estimate important physiological properties *in vivo*, such as the maximum rates of sarcoplasmic reticulum (s.r.) Ca^{2+} release and re-uptake, the voltage and time dependence of s.r. Ca^{2+} release, the possible inhibitory role of $\Delta[Ca^{2+}]$ on Ca^{2+} release and the time course of binding of Ca^{2+} to the regulatory sites on troponin C and the Ca^{2+}–Mg^{2+} sites on parvalbumin.

Although, in general, the muscle absorbance signals are relatively easily measured and have large signal-to-noise ratios, their quantitative interpretation cannot yet be

considered well established. For example, examination of properties of the dye signals, such as their wave-length and polarization dependence (Baylor *et al.* 1982*b*) and comparative time courses (Palade & Vergara, 1981, 1982; Baylor, Quinta-Ferreira & Hui, 1983; Quinta-Ferreira, Baylor & Hui, 1984*a*; Baylor, Hollingworth, Hui & Quinta-Ferreira, 1985), as well as measurements of *in vitro* dye binding to muscle components (Beeler, Schibeci & Martonosi, 1980) and diffusion constants within the myoplasm (Irving *et al.* 1985), have raised questions about the molecular mechanisms underlying the absorbance changes and the quantitation of the signals in terms of $\Delta[Ca^{2+}]$.

The experiments described in this paper were undertaken to characterize further the myoplasmic signals from Arsenazo III and Antipyrylazo III in intact (as opposed to cut) muscle fibres, with a view towards increasing the confidence with which quantitative physiological conclusions may be drawn from the dye signals. Because relatively little information was available about Antipyrylazo III signals from intact fibres, a major aim of these experiments was to characterize the muscle signals from Antipyrylazo III. During the course of the experiments, the new family of 'tetracarboxylate' Ca^{2+} indicator dyes designed and synthesized by R. Y. Tsien (Tsien, 1980, 1983) became available. These dyes have theoretical advantages over Arsenazo III and Antipyrylazo III in that they have the simplest possible Ca^{2+}–dye stoicheiometry (namely one Ca^{2+} to one dye molecule) and are much less sensitive to changes in pH and the Mg^{2+} concentration. It was therefore of interest to test at least one of the tetracarboxylate indicators in muscle under conditions identical to those used for the other two dyes. The dye chosen, Azo1 (Tsien, 1983), was selected because it undergoes an absorbance change in the visible region of the spectrum upon binding Ca^{2+} and it could be obtained in sufficient quantity to carry out a series of cuvette calibrations and muscle experiments.

The focus of this paper is on the properties of myoplasmic dye signals detected from fibres in the resting state. The main information to be obtained from resting fibres concerns: (i) the values of the diffusion constants of the dyes in myoplasm and whether they agree with expectations based on the assumption of physical (but not chemical) restrictions on the mobility of the molecules and (ii) the wave-length and polarization dependence of the signals and whether these properties agree with expectations from cuvette calibrations. For example, when compared with cuvette calibrations, the shape of the muscle absorbance spectra of Arsenazo III and Antipyrylazo III should give information about the myoplasmic free magnesium concentration, $[Mg^{2+}]$. More generally, a characterization of the dye signals in resting fibres is a necessary preliminary step for a quantitative understanding of the dye signals detectable during fibre activity.

An important conclusion that follows from the measurements is that, while the over-all pattern of the dye signals from resting fibres is now well characterized, a number of complex features have been detected. Taken together, these features suggest that under most recording conditions a large fraction, possibly a majority, of the dye molecules are not free in the myoplasmic solution and therefore not available to sense ionic activity in a straightforward manner. If so, a quantitative interpretation of the dye signals, either steady-state or transient, is rendered difficult unless a method is available for estimating the concentration of bound dye molecules

and characterizing their properties. It is concluded that, pending the availability of this information, quantitative inferences about $[Mg^{2+}]$ and $[Ca^{2+}]$ based on any of these, and probably other, metallochromic dyes should be made with caution, both in muscle and in other preparations.

Preliminary accounts of some of the results have appeared (Baylor, Quinta-Ferreira & Hui, 1985; Hollingworth & Baylor, 1986).

METHODS

The experiments were carried out in the Department of Physiology at the University of Pennsylvania using procedures similar to those described in Baylor *et al.* (1982*a*). Intact single twitch fibres were dissected from leg muscles (semi-tendinosus or iliofibularis) of English frogs (*Rana temporaria*) and mounted on an optical bench apparatus (Baylor & Oetliker, 1977) for the measurement of transmitted light intensities as a function of wave-length (λ) and polarization. In order to minimize movement artifacts in the optical records, the fibres were stretched to a long sarcomere spacing (3·4–4·5 μm) and lowered onto glass pedestal supports. The bath contained a normal Ringer solution (in mM: NaCl, 120; KCl, 2·5; $CaCl_2$, 1·8; Na_2PIPES (sodium salt of piperazine-*N*,*N*′-bis(2-ethane-sulphonic acid), 5) titrated to pH 7·10. The temperature of the bath was maintained at 16 °C ± 1 by a Peltier cooling system and was monitored in each experiment by means of a thermistor. Dye was pressure-injected into the myoplasm following penetration with a micropipette containing a filtered solution (pore size 0·22 μm) of distilled water plus 10–30 mM-dye. Fibre activity was triggered by action potential stimulation set up by a brief (< 1 ms) localized shock from a pair of extracellular electrodes positioned approximately 1 mm from the injection site.

A few new features were incorporated into the experimental arrangement.

(*i*) *Optics.* As previously reported (Baylor *et al.* 1982*a*) the fibre was illuminated with an unpolarized beam of quasi-monochromatic light, the wave-length of which was selected to be between 400 and 850 nm by first passing the beam through a heat filter (KG-1; Fish-Shurman, New Rochelle, NY, U.S.A.) and then an interference filter of either 'narrow' band (10 nm half-width; Ditric Optics, Hudson, MA, U.S.A.) or 'wide' band (30 nm half-width; Omega Optical, Brattleboro, VT, U.S.A.). After the light had passed through a field diaphragm of adjustable size, it was focused onto and collected from the fibre by means of two identical long-working-distance objectives (Leitz no.1569109; 32 ×, N.A. 0·6). An adjustable aperture diaphragm fitted to the back of the condensing objective was used to limit the N.A. of the incident light to 0·2–0·3 (Baylor *et al.* 1982*a*). At the level of the fibre, the beam usually consisted of a circular spot, 27–73 μm in diameter, selected in proportion to the fibre diameter, which varied in the range 35–120 μm. In order to increase the accuracy of the measurements of polarized absorbance, two identical silicon diode photodetectors were used, one of which measured the light intensity polarized parallel to the fibre axis, denoted 0 deg, and the other of which measured the light intensity polarized perpendicular to the fibre axis, denoted 90 deg. For this purpose a Thompson calcite beam-splitting prism (16 mm aperture; Karl Lambrecht Corporation, Chicago, IL, U.S.A.) was positioned behind the collecting objective on the optical bench. This prism allowed the 90 deg light to pass undeviated to the first photodetector while diverting the 0 deg light (at an angle of 45 deg to the undeviated beam) to the second photodetector. The voltage outputs of the photodetectors, which were linearly proportional to the light intensity, could then be sampled essentially simultaneously (see below) by the computer-controlled multiplexer and analog-to-digital converter, thus eliminating the need to make sequential (and time-bracketed) measurements with the two polarized forms.

(*ii*) *Data acquisition.* All data were digitally sampled, stored and analysed using a PDP 11/34 computer (Digital Equipment Corporation, Maynard, MA, U.S.A.) and a 12-bit analog-to-digital converter (model DT1711, Data Translation, Incorporated, Marlboro, MA, U.S.A.). Multiplexed input from six channels was collected in nearly all experiments.

(1) the intensity of 90 deg transmitted light prior to stimulation;
(2) the intensity of 0 deg transmitted light prior to stimulation;
(3) changes in 90 deg transmitted light intensity as a result of stimulation;
(4) changes in 0 deg transmitted light intensity as a result of stimulation;

(5) changes in fibre tension as a result of stimulation;
(6) the stimulating voltage applied to the external electrodes.

Prior to sampling by the analog-to-digital converter, channels 1 and 2 were led through unity gain operational amplifiers, whereas channels 3–6 were led through variable gain instrumentation amplifiers (model AM502, Tektronix, Incorporated, Beaverton, OR, U.S.A.). Additionally, channels 3 and 4 were led through sample-and-hold units that allowed for automatic subtraction of the resting light intensities (Baylor *et al.* 1982*a*) so that small changes in intensity could be measured more accurately.

A programmable stimulator (Page Digital Electronics, Duarte, CA, U.S.A.). served as a master timer for opening a shutter in the light path, gating the stimulus voltage, and controlling a data collection run, which usually consisted of the following: sampling of channels 1 and 2 prior to shutter opening; re-sampling of channels 1 and 2 after shutter opening; periodic sampling of channels 3–6 until 1000 samples had been collected from each channel. The difference between the measured intensities with shutter open and shutter closed provided the raw intensity values for calculating the resting fibre absorbances (see below). The 1000 sample points provided the raw data for determining changes in the fibre absorbance during fibre activity (Baylor *et al.* 1985). Stimulation of the fibre to give an action potential occurred at the time of the 80th sampling point. Following completion of a data-collection run at one wave-length, the interference filter was changed manually and the run repeated at a different wave-length. Bracketing runs at a particular wave-length were then periodically repeated during the course of the experiment. The time at which each record was taken was recorded automatically by means of the computer clock. The time between data-collection runs at different wave-lengths was typically 0·5 min (usual range 0·3–1·0 min).

(*iii*) *Dye injections.* Purified dyes were obtained from Sigma Chemical Co., St. Louis, MO, U.S.A. (Arsenazo III); ICN K and K Labs, Plainview, NY, U.S.A. (Antipyrylazo III); and as a generous gift from Dr R. Y. Tsien (Azo1). Although Arsenazo III can be injected easily into the myoplasm by means of ionophoresis (Miledi *et al.* 1977; Baylor *et al.* 1982*a*), pipettes filled with the other two dyes rarely passed significant quantities of dye into the myoplasm even though they readily passed a hyperpolarizing current following impalement of the fibre. Therefore, in nearly all of the experiments, including the Arsenazo III experiments, dye was injected into the myoplasm by means of pressure applied to the back of a moderately blunt micro-electrode, the resistance of which measured 40–100 MΩ when filled with dye (or approximately 2–5 MΩ if filled with 3 M-KCl). Following a successful penetration, the fibre region near the impalement site could be observed slowly and steadily, or in some cases dramatically, to colour with dye. Injections were typically completed within 0·5–5 min after impalement.

Three problems were encountered that collectively greatly reduced the probability of obtaining a successful injection. First, many pipettes (primarily those filled with Antipyrylazo III or Azo1) would pass dye for only a few seconds in the bath and then stop passing dye coincident with the visual appearance of a plug or 'crystal' of dye at the pipette tip. Secondly, higher-resistance pipettes that steadily passed dye in the bath often 'plugged' immediately upon impalement of the fibre. Alternatively, if a lower-resistance pipette was used, so that a larger amount of dye passed in the bath and plugging became less likely, fibre impalements often led to obvious damage to the membrane and/or uncontrollably large dye injections, accompanied by rapid swelling underneath the membrane at the impalement site. Thirdly, a number of fibres on which apparently successful injections were completed, gave graded rather than all-or-nothing optical and mechanical responses immediately after withdrawal of the pipette. A significant fraction of these fibres, however, recovered their normal all-or-nothing response (often rather abruptly) within 10–30 min following the injection. In most cases these fibres continued to respond to stimulation in an all-or-nothing manner for up to several hours after the injection, as did the fibres in which no functional indication of damage was detected immediately after completion of the injection. Results are reported in this paper only from fibres that gave stable, all-or-nothing optical and mechanical responses over periods of time lasting from many tens of minutes to several hours after injection. An additional requirement for the acceptance of a dye-injected fibre for study was that it have a normal birefringence signal (second component of Baylor & Oetliker, 1977), i.e. one of peak amplitude $1–3 \times 10^{-3}$ and a time-to-peak of 9–12 ms following the stimulating shock (at 16 °C).

(*iv*) *In vitro calibrations.* An important question in assessing the intracellular behaviour of any dye signal is whether its wave-length dependence is identical with that obtained in a calibrating

solution designed to mimic the main ionic features of the intracellular environment. For this purpose *in vitro* dye absorbance spectra were measured as described in Hollingworth & Baylor (1986) in 2–5 nm wave-length increments on a U.V.-visible spectrophotometer (model 4050, LKB Instruments). The standard calibrating solution consisted of 140 mM-KCl, 10 mM-K_2PIPES titrated to pH 6·90 with KOH, and variable additional amounts of Mg^{2+} and/or Ca^{2+} as specified in the Figure legends.

(*v*) *Optical bench calibrations.* In addition, checks were also made to assess the accuracy with which the *in vitro* dye spectra measured in a cuvette by the spectrophotometer agreed with that of the same solution as measured in a small-diameter glass capillary mounted in the position of a fibre on the optical bench. As described in connexion with Fig. 1, two sources of error were detected in the optical bench measurements, with respect to which all fibre measurements have been corrected.

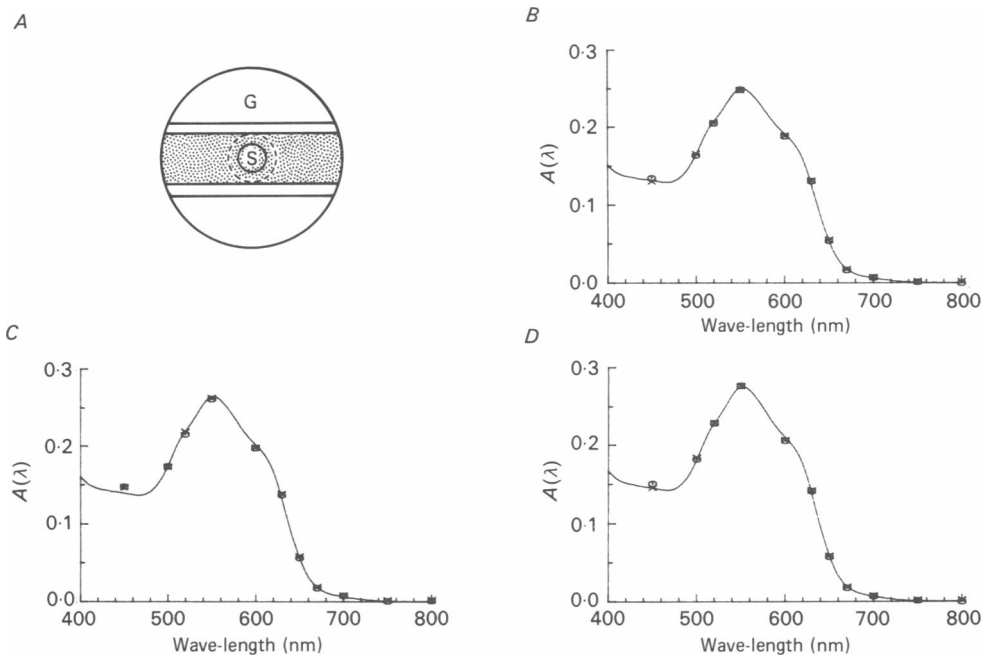

Fig. 1. Method for evaluating the accuracy of dye absorbance measurements on the optical bench apparatus. *A*, schematic diagram of dye-filled capillary as viewed on the optical bench. The 300 μm diameter field seen by the collecting objective includes a dye-filled capillary (shaded region) of i.d. 90 μm and o.d. 140 μm; the spot of light, S, of diameter 57 μm, used for measuring dye absorbance; and the background (unshaded) region, G, which includes some scattered and diffracted light, cumulatively referred to as glare, that interferes with the measurement of absorbance. The larger, dashed circle (diameter, 80 μm) represents the position of the secondary apertures placed in the objective image plane for the measurements shown in *C*. *B–D*, three methods for calculating the absorbance spectrum of the dye in the capillary. The estimated dye-related absorbances ($A(\lambda)$) obtained with 0 deg polarized light (circles) and 90 deg polarized light (crosses) are plotted as a function of the wave-length in nanometres. The continuous curves are three scalings of a single absorbance spectrum of the dye measured in a cuvette in the spectrophotometer. In each case the scaling is appropriate for comparison with the calculated capillary absorbance: *B*, absorbance calculated from measurements without secondary aperture and without correction for glare ($g = 0{\cdot}0$ in eqn. (3)); *C*, absorbance calculated from measurements with the secondary apertures and without correction for glare; *D*, absorbance calculated from measurements without the secondary apertures but with correction for glare ($g = 0{\cdot}075$ in eqn. (3)). See text for details.

Fig. 1*A* shows a representation, approximately to scale as viewed on the optical bench, of a portion of a thin-walled glass capillary filled with the standard calibrating solution plus 1·2 mM-Antipyrylazo III. The inner diameter (i.d.) of the capillary was approximately 90 μm and the outer diameter (o.d.) approximately 140 μm. The small circle S represents the reduced image of the field aperture diaphragm focused in the middle of the capillary. This circle of light appeared visually as a single bright spot and supplied the transmitted intensity by means of which the (apparent) absorbance of the dye, A, may be measured using the equation:

$$A = \log_{10}(J/I), \tag{1}$$

where J is the total light intensity measured by the photo-detector when the capillary contains a blank solution (calibrating solution without dye) and I is the intensity measured in the presence of the dye-containing solution. Fig. 1*B* shows the 0 deg apparent absorbance (circles) and 90 deg apparent absorbance (crosses) of the dye in the capillary calculated as a function of wave-length between 450 and 800 nm, as selected by the 10 nm interference filters. As expected for molecules in free solution, there was no detectable dichroism in the measurements, as the 0 deg and 90 deg absorbance values essentially superimpose at all wave-lengths. For comparison, the smooth curve in Fig. 1*B* is the absorbance of the same solution measured in the spectrophotometer in a 500 μm path-length cuvette. This curve has been scaled by the factor 0·154 to give a least-squares best fit to the capillary measurements. It should be noted that there is essentially no difference between the spectral shapes as determined in the spectrophotometer and on the optical bench. There was, however, a difference between the expected amplitude of the scaling factor and that which was used: the expected amplitude, which, according to the simplest estimate, would be given by the ratio of the path lengths, 90/500 = 0·180, was some 16·9 % larger than the best-fit scaling employed for the data in Fig. 1*B*.

The first correction that needed to be applied to reconcile the optical bench measurements with the spectrophotometer measurements arises from the fact that the spot S is not of infinitely small diameter. Thus the path length through the capillary is, in fact, equal to the full capillary i.d. only at the very centre of the capillary. Towards the periphery the path length through the capillary is necessarily smaller than the i.d. Based on simple geometric considerations, it is possible to estimate a correction factor p which relates the light path length averaged over the area of the spot to the path length at the middle of the spot, according to the equation:

$$p = \frac{4}{\pi f^2}\int_0^f \sqrt{(f^2-y^2)}\sqrt{(1-y^2)}\,dy, \tag{2}$$

where f is the ratio of the spot diameter to the capillary (or fibre) diameter. For the situation of Fig. 1*B*, $f = 57/90$ and therefore $p = 0{\cdot}947$. Hence, a somewhat smaller scaling factor of $(90 \times 0{\cdot}947)/500 = 0{\cdot}170$ (rather than 0·180) would be expected in order to relate the amplitude of the spectrophotometer measurements to that of the optical bench measurements in Fig. 1*B*. However, the number 0·170 is still some 10·4 % larger than the observed best-fit scaling factor, 0·154.

The major additional source of error in the optical bench measurements is supposed to arise in the following way. In Fig. 1*A* light within the region of spot S is the principal but not the exclusive source of intensity measured by the photodetector. In particular, some light, due to a combination of scattering and diffraction, passes around the capillary (in the 'glare' region labelled G in Fig. 1*A*) rather than through the capillary, where it is subject to dye absorbance. The presence of any such light will clearly make the use of eqn. (1) inaccurate. That some glare-related error of this sort must exist was confirmed by visual observation, which revealed that region G, while quite dark, was not completely black.

The following equation is therefore assumed to give a more accurate estimate of the dye absorbance A (in the capillary or fibre) as measured on the optical bench:

$$A = \log_{10}(J-gJ)/(I-gJ), \tag{3}$$

where g gives the fraction of the intensity J that is measured by the detector in the absence of dye but that does not pass through the capillary (or fibre) and is therefore not susceptible to dye absorbance. Clearly, eqn. (1) is a special case of eqn. (3) for the situation where all the incident intensity is subject to dye absorbance ($g = 0$).

Two methods were used to estimate the magnitude of the parameter g in eqn. (3). The first method was to use a pair of secondary spots (diaphragms) placed in front of the 0 deg and 90 deg photo-

detectors in the objective image plane so as to mask out the stray light from the glare region. The location of these spots relative to the usual image 'seen' by the photodetectors is indicated by the dashed circle in Fig. 1*A*. With the secondary spots in place, the parameter g in eqn. (3) should be close to zero, so that little error should arise by simply using eqn. (1). Measurements of capillary dye absorbance using this technique and calculated by eqn. (1) are shown as the data points (circles and crosses) in Fig. 1*C*. For comparison, a best fit to these data of the absorbance curve measured by the spectrophotometer is also shown (continuous curve), where the scaling factor in this case was 0·163. If it is assumed that the bench absorbance measurements in Fig. 1*C* are correct, the analogous data set in Fig. 1*B* may be made to superimpose the correct values if eqn. (3) is used with the parameter g taken as an adjustable parameter. In this case a best fit is obtained if the glare parameter $g = 0{\cdot}045$ at 550 nm. At other wave-lengths λ, $g(\lambda)$ is assumed to be given by:

$$g(\lambda) = g(550) \times (550/\lambda). \tag{4}$$

The use of a λ^{-1} dependence for $g(\lambda)$, rather than some higher or lower exponent, was justified by a separate analysis of the λ dependence of the data set which related the fraction of the light excluded by the secondary spots in the absence of a capillary to the illuminating wave-length. It may be noted that this estimate of $g(550) = 0{\cdot}045$ does not depend directly on measurements of path length (in particular the ratio of path length in the capillary to path length in the cuvette) or on the factor p, both of which may be subject to small errors.

The second estimate of g was obtained using the assumption that there are no errors in the measurement of the ratio of path lengths (= 90/500) or in the correction factor p (= 0·947) obtained from eqn. (2). Under this assumption the raw intensity values measured in connexion with Fig. 1*B* may be analysed using eqn. (3) and the value of g adjusted until a best fit of optical bench absorbance is obtained relative to the curve shown in Fig. 1*D*. This curve is the spectrophotometer absorbance curve scaled by the factor 0·170 (= 0·947 × 90/500). Based on this approach, the resulting fit gave $g = 0{\cdot}075$ at 550 nm, a value in fair agreement with the value 0·045 obtained by the first method for estimating g. Hence, the final procedure adopted in this paper for the conversion of raw intensity measurements to absorbance units was to use eqns. (3) and (4) with a value of g at 550 nm of 0·06, the average of 0·045 and 0·075.

It should be emphasized that the main effect of using eqns. (3) and (4) rather than eqn. (1) is to introduce a relatively small increase in the estimate of the amplitude of absorbance but not a significant change in spectral shape (see Fig. 1*B–D*). Moreover, the choice of eqns. (3) and (4) over eqn. (1) does not introduce any dichroism into the estimates of dye absorbance (see Fig. 1*B–D*). Thus, conclusions in this paper regarding the existence of muscle dye spectra that differ in spectral shape from cuvette calibrations, or that reveal dichroic components, do not depend on the exact method for estimating dye absorbance on the optical bench. However, given the uncertainties in the above estimates, the accuracy of the absolute amplitude of the muscle absorbance values is probably no better than about ±3%.

In many cases the absorbance measurements have also been referred to dye concentration units, c, by means of Beer's law:

$$c = A/(\epsilon l), \tag{5}$$

where ϵ is the molar extinction coefficient of the dye and l is the effective path length of light in the myoplasmic solution. For this purpose it was assumed that

$$l = 0{\cdot}7\ pd, \tag{6}$$

where the factor 0·7 gives the estimated fraction of the fibre volume occupied by the myoplasmic solution (Baylor *et al.* 1983); p is the correction factor given in eqn. (2); and d, the fibre diameter, was estimated as given in Baylor *et al.* (1982*a*) from measurements of the resting birefringence and the fibre diameter as viewed in the direction perpendicular to the light path. The following values were used for molar extinction coefficients: for Arsenazo III, $\epsilon(570\text{ nm}) = 3{\cdot}0 \times 10^4\ \text{M}^{-1}\ \text{cm}^{-1}$ (Baylor *et al.* 1982*a*); for Antipyrylazo III, $\epsilon(550\text{ nm}) = 2{\cdot}7 \times 10^4\ \text{M}^{-1}\ \text{cm}^{-1}$ (see Appendix); and for Azo1, $\epsilon(480\text{ nm}) = 2{\cdot}57 \times 10^4\ \text{M}^{-1}\ \text{cm}^{-1}$ (Tsien, 1983; Hollingworth & Baylor, 1986).

An additional, practical limitation to the accuracy of the absorbance measured in the experiments is related to the long-term stability of the light source. Typically, a complete spectral run, in which light intensities I were measured over an extended series of wave-lengths, was made without moving the fibre from its position in the illuminating beam. This run was either preceded or followed, or

in many cases both preceded and followed, by another spectral run with the fibre removed from the beam of light. These latter measurements gave the light intensities J for use in eqn. (3). Since the I values and J values were determined at different times, typically 10–30 min apart, it was important that lamp drift be kept as small as possible. This was achieved by allowing a long warm-up period for the lamp, which was usually turned on 2–3 h before an experiment was started. In this situation, the drift in J values over a 10–30 min period was typically $\pm 0{\cdot}5\,\%$, corresponding to an uncertainty in absorbance units of $\pm 0{\cdot}002$ ($= 0{\cdot}005/\log_e 10$). Results from experiments in which the lamp showed evidence of long-term instability, or in which the I and J values were not determined within a reasonable time of each other (e.g. less than 45 min), have not been included in the analysis.

Computer simulation of diffusion with binding

The analysis carried out in connexion with Fig. 12 required the simulation by computer of the process of longitudinal dye diffusion in the presence of saturable myoplasmic binding sites. As described in the Results (see pp. 127–128), the initial profile giving the total Antipyrylazo III concentration as a function of the distance x from the injection site, $[A_t](x)$, was assumed to satisfy the right-hand side of eqn. (16), the equation for one-dimensional diffusion of an impulse of dye away from a point source. The main technical problem encountered in calculating the spatial profile at either earlier or later times by means of eqns. (18)–(20), the equations for diffusion with saturable binding, was the finding that the profile became unstable (very noisy) after a relatively small number of integration steps, i.e. that in total it covered only a fraction of the over-all time required for the simulation. This problem presumably arose because of the noise inherent in the process of taking second derivatives of $[A_t](x)$ as required by eqn. (18). Thus, in order to continue the simulation it was necessary periodically to 'smooth' the function $[A_t](x)$ as it advanced in time. Although the fitting of a general functional form to $[A_t](x)$ might have been employed for this purpose, it was found that eqn. (16) itself gave an excellent empirical fit to the simulated profile at all times of interest. This circumstance should probably not be regarded as entirely fortuitous, since it is presumably related to the experimental finding that measured dye profiles were always well described by eqn. (16), even when the apparent diffusion constant, D_{app}, progressively changed with time (see Fig. 11). Therefore, the procedure adopted was repeatedly to apply eqns. (18)–(20) to advance the integration in time until the point was reached at which the profile $[A_t](x)$ was in danger of becoming too noisy, then stop the integration and do a least-squares fit of eqn. (16) to $[A_t](x)$, adjusting the parameters M and D_{app}, then replace the profile by that calculated from the fit of eqn. (16), and finally re-apply eqns. (18)–(20) to advance the integration. The function $[A_t](x)$ itself was calculated in 6 μm increments, between -1500 μm and $+1500$ μm from the site of dye injection. For the calculation of the first and second derivatives with respect to x, a five-point differentiation 'filter' (Hamming, 1977, p. 107) was used. The over-all accuracy of the simulation was tested by applying the procedure to one-dimensional diffusion without binding, and calculating, as a function of time, the values of D_{app} that gave a best fit to the simulated profiles. In this case the value of D_{app} was expected to remain constant, and did so with an error of less than 5 % over the time of the integration. A similar maximum error of 5 % is thought to apply to the theoretical curves shown in Fig. 12*A*.

RESULTS

In order to estimate dye-related signals from fibres injected with dye, it is necessary to subtract from the measured total fibre absorbance the contribution due to 'intrinsic,' i.e. non-dye-related, absorbance. The approach adopted for making the intrinsic correction was similar to that given in Baylor *et al.* (1982*a*). However, a somewhat more detailed investigation into the wave-length and polarization dependence of the intrinsic signals was carried out here so that the muscle dye signals might be resolved as accurately as possible.

Intrinsic absorbance in resting fibres

As shown in Baylor *et al.* (1982*a*), the intrinsic absorbance of a single fibre measured

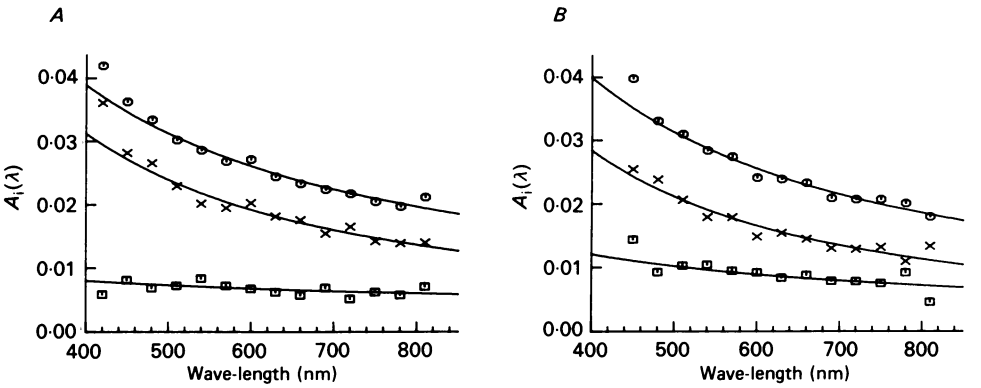

Fig. 2. Intrinsic absorbance $A_i(\lambda)$ (ordinate) for two fibres (A, B) plotted as a function of wave-length (abscissa) for 0 deg (circles) and 90 deg (crosses) polarized light. The intrinsic dichroic absorbance, i.e. $A_0(\lambda) - A_{90}(\lambda)$, is also shown (rectangles). The continuous curves are least-squares fits of eqn. (7) to the various data sets. A, fibre no., 061182·1; sarcomere spacing, 4·0 μm; 17 °C. For the three fits the exponential index X in eqn. (7) was 0·99 (0 deg), 1·20 (90 deg) and 0·41 (dichroic). B, fibre no. 070282·11; sarcomere spacing, 3·9 μm; 16 °C. For the three fits the exponential index was 1·10 (0 deg), 1·32 (90 deg) and 0·74 (dichroic). (See Table 1 for fibre diameters, spot sizes, etc.)

with unpolarized light decreases with wave-length and approximately follows a $1/\lambda$ dependence. The measurements illustrated in Fig. 2 and summarized in Table 1 were carried out to describe this wave-length dependence more accurately and to extend the description to both 0 deg and 90 deg polarized absorbances.

Fig. 2A shows the results from one fibre in which absorbance as a function of wave-length was measured in 30 nm steps between 420 and 810 nm using both 0 deg (circles) and 90 deg (crosses) polarized light, where $A_0(\lambda)$ is the absorbance measured with 0 deg light and $A_{90}(\lambda)$ is the absorbance measured with 90 deg light. Also plotted at each wave-length in Fig. 2A is the intrinsic dichroic absorbance, i.e. the difference between the absorbances of the two polarized measurements (rectangles). For both polarizations the absorbance values were calculated using eqns. (3) and (4), with the reference intensity values, $J(\lambda)$, determined after removal of the fibre from the optical path (see Methods).

The continuous curves in Fig. 2A all follow the same functional form:

$$A(\lambda) = c\lambda^{-X}, \tag{7}$$

where $A(\lambda)$ is absorbance as a function of wave-length λ, and c and X are arbitrary constants. The particular curves shown are the least-squares best fits of eqn. (7) to each of the three data sets (excluding the 420 nm and 450 nm points) obtained by adjusting the parameters c and X. It is apparent that the data points in Fig. 2A are well described by eqn. (7) over the range 480–810 nm. At the two shorter wave-lengths, however, the measurements appear to rise more steeply with wave-length than the curves themselves. A reasonable fit to the complete data sets, i.e. including the 420 and 450 nm points, can also be obtained using eqn. (7); however, in this case the fit to the longer wave-length data is slightly less good. Because the principal

wave-length range to be analysed in fibres injected with Arsenazo III or Antipyrylazo III was 480–810 nm, the analysis of the intrinsic absorbance data has been restricted here to $\lambda \geqslant 480$ nm. Similar data and satisfactory empirical fits are shown in Fig. 2*B* for a second fibre.

Table 1 summarizes the results of this type of analysis applied to six runs from five different fibres, all of which were satisfactorily fitted by eqn. (7). In each case the absorbances at 0 deg were larger than the absorbances at 90 deg, whereas the exponential index X in eqn. (7) for the 0 deg data (X_0) (column (6) of Table 1) was less than or equal to that for the 90 deg data (X_{90}) (column (7) of Table 1). On average, X_0 was 1·1 and X_{90} was 1·3. (As expected from the finding that $X_0 < X_{90}$, the exponential index for the fits to the dichroic data, which are not shown in Table 1, was smaller, being on average 0·5.) For fibres injected with Arsenazo III and Antipyrylazo III the following equations were therefore adopted for estimating the value of the intrinsic absorbance at wave-length λ, $A_i(\lambda)$, which must be subtracted from the total fibre absorbance in order to estimate the dye-related absorbance:

$$A_{i,0}(\lambda) = A_0(\lambda_{long})(\lambda_{long}/\lambda)^{1.1}, \tag{8}$$

$$A_{i,90}(\lambda) = A_{90}(\lambda_{long})(\lambda_{long}/\lambda)^{1.3}, \tag{9}$$

where $A_{i,0}(\lambda)$ is the intrinsic absorbance measured with 0 deg light, $A_{i,90}$ is the intrinsic absorbance measured with 90 deg light and λ_{long} refers to a wave-length beyond the absorbance band of the dye where intrinsic absorbance alone is detected (for example, 810 nm for Antipyrylazo III, 750 nm for Arsenazo III).

An analogous correction was applied to the absorbance of fibres injected with Azo 1. However, with this dye the principal absorbance range of interest was at considerably shorter wave-lengths, $\lambda < 650$ nm. Unfortunately, with the tungsten–halogen bulb used for the experiments, lamp intensities fall off steeply below 480 nm. Therefore, measurements of fibre resting absorbance below 480 nm are less reliable. Nevertheless, in order to maximize the information available from the Azo 1-injected fibres, it was of interest to re-analyse the intrinsic absorbance measurements for the fibres in Table 1 using the wave-length range $450 \leqslant \lambda \leqslant 630$ nm. The data were again well fitted using eqn. (7), although the exponential index X for the 90 deg data was slightly larger, on average 1·5 rather than 1·3. The 0 deg exponential index, however, was unchanged. For estimation of the intrinsic absorbance in Azo 1-injected fibres, eqn. (9) was therefore modified to use the larger exponent, 1·5. The value of λ_{long} selected for the Azo 1 measurements fell between 600 and 630 nm.

Although the empirical description of intrinsic absorbance in any given fibre is well fitted by eqn. (7), it must be kept in mind that the estimates of $A_i(\lambda)$ in a dye-injected fibre obtained by means of eqns. (8) and (9) are not as accurate as might be supposed from the good fits in Fig. 2, where the average deviation about the curves is less than 0·001 absorbance units. Rather, the uncertainty is significantly larger for two reasons. First, $A(\lambda_{long})$ was usually measured at only one wave-length (or in some cases, the average of two closely adjacent wave-lengths); thus some uncertainty is introduced because of the scatter associated with any given measurement. Secondly, some variation is expected between the mean exponential absorbance indices for the population of fibres (1·1 for 0 deg, 1·3 for 90 deg) and the indices that apply to any particular fibre; this variation introduces additional uncertainty, even for a fibre

TABLE 1. Amplitude and wave-length dependence (480 nm $\leqslant \lambda \leqslant$ 810 nm) of polarized absorbance in non-injected fibres

Fibre no. (1)	Fibre diameter (μm) (2)	Spot diameter (μm) (3)	$A_0(810)$ (4)	$A_{90}(810)$ (5)	Exponent for $A_0(\lambda)$ (6)	Exponent for $A_{90}(\lambda)$ (7)	Average value of observed minus predicted		
							$A_0(\lambda)$ (8)	$A_{90}(\lambda)$ (9)	$A_0(\lambda)-A_{90}(\lambda)$ (10)
060882·1	54	30	0·0357	0·0288	1·16	1·38	−0·0008	−0·0017	0·0009
060982·1	73	43	0·0170	0·0153	1·34	1·34	−0·0006	−0·0035	0·0029
061182·1	65	43	0·0211	0·0140	0·99	1·20	−0·0031	−0·0014	−0·0017
070282·11	70	43	0·0180	0·0134	1·10	1·32	0·0005	−0·0030	0·0035
070282·12	70	43	0·0218	0·0145	1·14	1·48	0·0000	0·0001	−0·0001
112183·1	76	43	0·0172	0·0133	0·92	1·20	−0·0012	−0·0029	0·0017
Mean ($n = 6$)	—	—	0·0222	0·0163	1·11	1·32	−0·0009	−0·0021	0·0012
S.E. of mean	—	—	—	—	±0·06	±0·04	—	—	±0·001

The Table summarizes the results of fitting eqn. (7) in the text to measurements of absolute fibre absorbance in non-injected fibres. The measurements were made from five separate fibres, one of which (070282·1) had two runs taken approximately 45 min apart from two different fibre regions. In all cases, the absorbance data collected between 810 and 480 nm in 30 nm steps were analysed (12 points per run). Wide-band filters were used throughout. Column (1) gives the fibre identification number; column (2), the fibre diameter; column (3), the spot size used to make the measurements; columns (4) and (5), the values of the 0 deg and 90 deg absorbances measured at $\lambda = 810$ nm; columns (6) and (7), the values of X in eqn. (7), which give a best fit, respectively, to the data for the 0 deg absorbance and the 90 deg absorbance. Columns (8)–(10) give, respectively, for the 0 deg, 90 deg and dichroic data, the average deviation ($\lambda < 810$) between the measured absorbance and that predicted by eqn. (7) if the population averages of X are applied to the measured values of $A(810)$.

which might have a completely accurate measurement of $A(\lambda_{long})$. An attempt to evaluate the over-all uncertainty is given in Table 1, columns (8)–(10). For each run shown in the Table, $A_i(\lambda)$ was estimated at each wave-length less than 810 nm, using eqns. (8) and (9), and the measured value of $A(810\,nm)$ for that run. This 'predicted' value was then subtracted from the measured value of $A_i(\lambda)$ and the average deviation ($480\,nm \leqslant \lambda \leqslant 780\,nm$) was tabulated separately for the 0 deg, 90 deg and dichroic data. These values, which ranged up to 0·004 absorbance units, are presumed to give a more accurate indication of the uncertainty involved in correcting for fibre intrinsic absorbance. (A significant fraction of this uncertainty may be attributed to the long-term drift in the lamp intensity, see Methods.) The average absolute value of this deviation for the six runs in columns (8)–(10), 0·001–0·002, would suggest that any particular dye-related effect would have to be at least as large as 0·003–0·004 absolute absorbance units before being considered as possibly reliable.

The reproducibility of measurements of the type shown in Table 1 and Fig. 2 was checked in one of the fibres, fibre 070282·1. Results essentially superimposable with those shown in Fig. 2*B* were obtained when: (i) the absorbances were simply re-measured at the same location using the same (43 μm) spot size; (ii) the absorbances were re-measured at the same location using a different (57 μm) spot size; and (iii) absorbances were re-measured using narrow-band rather than wide-band filters (43 μm spot size). These results indicate that the adequacy of the description of intrinsic absorbance given by eqns. (8) and (9) is not limited in other fibres by the exact choice of fibre location, spot size, type of filter, and λ_{long}.

Absorbance of Arsenazo III in resting fibres

A piece of information of general importance in evaluating the intracellular behaviour of any indicator dye is its resting spectrum measured as a function of polarized light. For example, if the entire population of dye molecules is free within the cytoplasmic solution, polarized absorbance measurements should be identical (isotropic), since molecules in solution should be able to orient to all directions with equal probability. In this case, the spectrum of the dye compared with cuvette calibrations should give information about the ionic conditions of the myoplasm. For example, for Arsenazo III the resting absorbance spectrum should mainly reflect the resting levels of pH and free $[Mg^{2+}]$, since resting $[Ca^{2+}]$ is negligibly small compared with the effective dissociation constant of the dye for $[Ca^{2+}]$. Alternatively, if absorbance differences are detected as a function of polarized light (dichroism), a fraction of the dye molecules must be oriented, as a result, for example, of binding to oriented structures within the cytoplasm. In this case the isotropic spectrum must be interpreted with caution, since a dichroic signal which is only a small fraction of the isotropic spectrum might in fact reflect a much larger fraction of bound dye molecules (see below).

Information about the resting spectra of Arsenazo III in myoplasm was obtained from seven runs on five different fibres. An example of the measurements is shown in Fig. 3, from the fibre with the largest amount of injected dye and the most complete spectral run. The raw estimates of total fibre absorbance (intrinsic plus dye-related) are shown in Fig. 3*A* for both 0 deg (circles) and 90 deg (crosses) polarized light. For all wave-lengths, $A_0(\lambda)$ was greater than $A_{90}(\lambda)$, indicating the presence of a dichroic

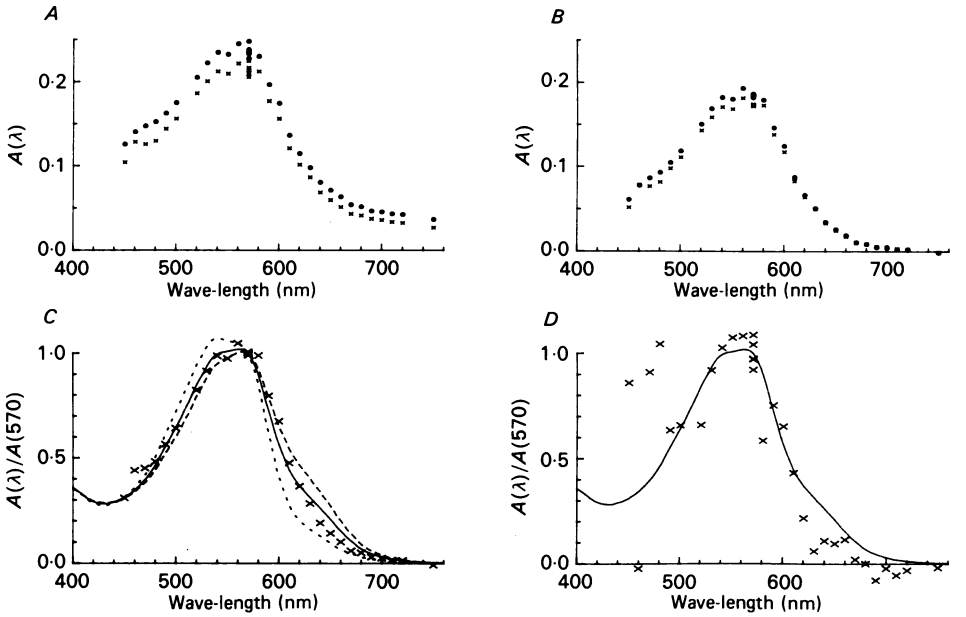

Fig. 3. Resting spectra from a fibre injected with Arsenazo III. *A*, absolute fibre absorbance (intrinsic plus dye-related) measured with 0 deg (circles) and 90 deg (crosses) polarized light. *B*, dye-related polarized absorbances A_0 (circles) and A_{90} (crosses), from the data in *A* after subtraction of intrinsic absorbance and normalization for the steady decrease in dye concentration during the run (see text). *C*, isotropic dye absorbance (crosses) obtained from spectra in *B* as $(A_0+2A_{90})/3$ and scaled so that $A(570) = 1{\cdot}0$. *D*, dichroic dye absorbance (crosses) obtained from spectra in *B* as (A_0-A_{90}) and scaled so that average $A(570) = 1{\cdot}0$. The curves in *C* and *D* are cuvette calibrations at a total dye concentration, $[D_t]$, of 1·6 mM, pH 6·9 and free $[Mg^{2+}]$ of 0 mM (dotted line), 2 mM (continuous line) and 4 mM (dashed line). Fibre no., 031 983·12; sarcomere spacing, 3·6 μm; 16·0 °C. The run was taken 50–70 min after dye injection. The average isotropic $A(570)$ of 0·18 corresponds to a total dye concentration, $[D_t]$, of 1·6 mM.

signal, some fraction of which is undoubtedly attributable to the intrinsic dichroic signal (Fig. 2). Fig. 3*B* shows the absorbance data after subtraction of the intrinsic component (eqns. (8) and (9)) and, in addition, after a normalization for variations in the total dye concentration, which decreased steadily during the run. For the latter normalization, the amplitude of the dye-related $A(570)$ was estimated at the time of each measurement of $A(\lambda)$, by interpolation over the range of the five measured values of $A(570)$. Each $A(\lambda)$ was then scaled by the ratio of the interpolated $A(570)$ present at the mid-point of the run divided by the interpolated $A(570)$ applicable to each measurement. Thus the concentration-adjusted amplitudes (Fig. 3*B*, which were normalized separately for each polarization) refer to the value of dye-related $A(570)$ present at the mid-point of the run (0·184 for the 0 deg absorbance, 0·173 for the 90 deg absorbance). According to eqns. (5) and (6), these latter absorbances correspond to an average dye concentration of 1·6 mM.

The spectral shapes in Fig. 3*B* are closely similar for both forms of polarized light, but the 0 deg absorbances are consistently larger than the 90 deg absorbances, on

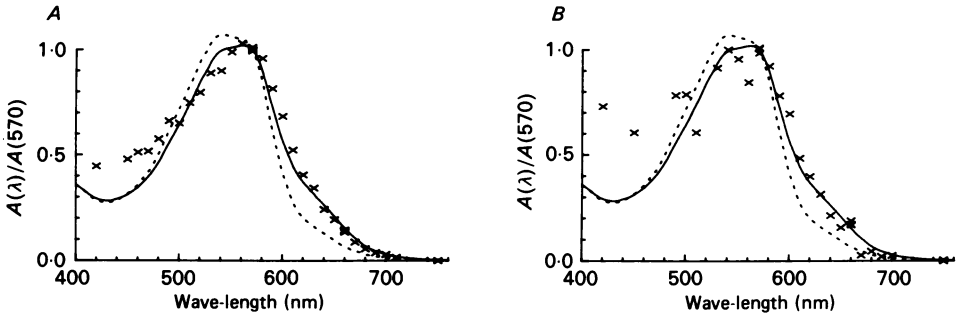

Fig. 4. Isotropic spectra (crosses) from two different fibres injected with Arsenazo III, obtained as described for Fig. 3*C*. The curves are cuvette calibrations at a $[D_t]$ of 2·0 mM, pH 6·9, and a free $[Mg^{2+}]$ of 0 mM (dashed line) and 2 mM (continuous line). *A*, fibre no., 111583·1; sarcomere spacing, 3·6 μm; 16 °C. The run was made 35–46 min after injection; average $A(570)$ during the run was 0·078, corresponding to a $[D_t]$ of 0·58 mM. *B*, fibre no., 070982·2; sarcomere spacing, 3·7 μm; 16 °C. The run was made 23–38 min after injection; average $A(570)$ during the run was 0·085, corresponding to a $[D_t]$ of 0·66 mM.

average about 6% larger. In absolute absorbance units this average difference was 0·011 at $\lambda = 570$ nm, a value considerably larger than the uncertainty associated with the intrinsic correction. This difference is therefore attributed to the presence of a small Arsenazo III resting dichroic signal (see the next section). Under the assumption that possible errors due to the presence of the dichroic signal may be ignored, it is of interest to calculate the 'isotropic' spectrum of Arsenazo III as an indication of the myoplasmic free $[Mg^{2+}]$. As discussed in Baylor *et al.* (1982*c*), the isotropic spectrum, calculated by the formula $(A_0 + 2A_{90})/3$, represents the average spectrum of all the dye molecules, independent of orientation. This spectrum may then be normalized by its average value at $\lambda = 570$ nm and its shape (crosses, Fig. 3*C*) compared with similarly normalized cuvette calibrations obtained as a function of free $[Mg^{2+}]$. The calibration curves shown in Fig. 3*C* were all obtained at pH 6·90 (the probable pH of the myoplasm under the conditions of the experiments; see Baylor *et al.* (1982*a*) but at three levels of free $[Mg^{2+}]$: 0, 2·0 and 4·0 mM. The over-all shape of the muscle spectrum is better fitted by the 2·0 mM-Mg^{2+} curve than the 0 or 4·0 mM-Mg^{2+} curves, which suggests that the free $[Mg^{2+}]$ in myoplasm is closer to 2·0 mM than to 0 or 4·0 mM if the resting pH is 6·90. (Alternatively, if the resting pH is 7·10, the data suggest that the resting free $[Mg^{2+}]$ is approximately 0·44 times the value indicated at pH 6·90; see the cuvette calibrations in Baylor *et al.* (1982*a*).)

Fig. 4 shows results from two other fibres, which were injected with considerably smaller dye concentrations, and for which the data were analysed in an identical fashion and the shapes of the Arsenazo III isotropic spectrum were compared with the same 0 and 2 mM-cuvette calibrations for $[Mg^{2+}]$. As in Fig. 3*C*, the data are closely similar to those of the 2·0 mM-Mg^{2+} curve throughout much of the wave-length range ($\lambda > 520$ nm). This agreement indicates that the spectral shape can be reproducibly determined using different fibres injected with a range of dye concentrations. The variation in shape that is apparent at shorter wave-lengths ($\lambda < 520$ nm), an effect probably attributable to the lower lamp intensities and a greater uncertainty

in the correction for intrinsic absorbance at these wave-lengths, suggests that the shorter wave-length data should probably be ignored in attempting to estimate the free $[Mg^{2+}]$.

A quantitative estimate of $[Mg^{2+}]$ may be made in the following way from data of the type shown in Fig. 3*C* and Fig. 4. The fraction of dye in the Mg^{2+}-bound form, f_{Mg}, is related to the free $[Mg^{2+}]$ by the equation:

$$f_{Mg} = [Mg^{2+}]/([Mg^{2+}]+K_{D,Mg}), \tag{10}$$

where $K_{D,Mg}$ is the apparent dissociation constant of the Mg^{2+}–Arsenazo III reaction and has been previously measured to be 6·2 mM at pH 6·9 (Baylor *et al.* 1982*a*). On the other hand, the normalized spectral shape $A(\lambda)/A(570)$ is related to f_{Mg} by the equation (see, for example, Baylor *et al.* 1982*a*, eqn. 12):

$$\frac{A(\lambda)}{A(570)} = \frac{\epsilon_0(\lambda)}{\epsilon_0(570)} + \frac{\Delta\epsilon_{max}(\lambda)}{\epsilon_0(570)} f_{Mg}, \tag{11}$$

where $\epsilon_0(\lambda)/\epsilon_0(570)$ is the normalized shape of the dye spectrum in a 0-Mg^{2+} environment (and is identical to the 0-Mg^{2+} curve in Fig. 3*C*) and $\Delta\epsilon_{max}(\lambda)/\epsilon_0(570)$ is the normalized shape of the spectral change that arises when all the dye switches to the Mg^{2+}-bound form. This latter shape is proportional to the difference between any two of the curves in Fig. 3*C*, and its absolute amplitude may be calculated directly by means of eqn. (10), for example by dividing the difference between the 2·0 mM-Mg^{2+} and the 0 mM-Mg^{2+} curves in Fig. 3*C* by 2·0/(2·0+6·2). Given this determination of the two theoretical shapes required by the right-hand side of eqn. (11), a linear least-squares fit to the data (considered as the left-hand side of eqn. (11)) may be made by adjusting the value of f_{Mg}. From f_{Mg}, the free $[Mg^{2+}]$ may be calculated by means of eqn. (10). The results of the application of this fitting procedure to the Arsenazo III resting spectral measurements (520 nm $\leqslant \lambda \leqslant$ 700 nm) are summarized in Table 2, columns (9) and (10). The results indicate that, on average, the myoplasmic free $[Mg^{2+}]$ is 2·3 mM if the pH is 6·90 (or 1·0 mM if the pH is 7·10). As shown in Fig. 5*A*, there appeared to be no significant correlation between the estimate of the free $[Mg^{2+}]$ and the concentration of Arsenazo III with which the estimate was made. This result is expected if the dye senses the $[Mg^{2+}]$ in a straightforward way, and if effects such as Mg^{2+} buffering by the dye itself are small.

The average value estimated for the $[Mg^{2+}]$, 2·3 mM, (±0·2 S.E. of mean), appears to be significantly larger than the average value, 1·2 mM (±0·3 S.E. of mean), determined by Baylor *et al.* (1982*a*), who made their measurements under closely similar experimental conditions but used spectral information at only two wave-lengths 530 and 650 nm. The difference between the present and the earlier results is not attributable to differences in the cuvette calibrations for Arsenazo III, which agree within a few per cent at the wave-lengths 530 and 650 nm. Rather, the difference is attributable to both the wave-length range selected for analysing the dye-related absorbance and the method chosen for removing the fibre intrinsic absorbance. In particular, at wave-lengths of 650–660 nm, where the difference between the two methods for estimating the intrinsic absorbance is small, the results are closely similar: 1·2 mM (±0·2 S.E. of mean) (Baylor *et al.* 1982*a*) and 1·0 mM (±0·2 S.E of mean) (average value for the seven runs in Table 2, not shown as a function of

TABLE 2. Analysis of Arsenazo III resting spectra for dichroism and the free $[Mg^{2+}]$

Fibre no. (1)	Fibre diameter (μm) (2)	Spot diameter (μm) (3)	No. of measurements (4)	$A(570)$ $(A_0+2A_{90})/3$ (5)	$[D_t]$ (mM) (6)	Fractional dichroic amplitude (7)	Oriented dye concentration (μM) (8)	f_{Mg} (9)	$[Mg^{2+}]$ (mM) (10)
061282·21	35	27	14	0·117	1·72	0·056	32	0·256	2·13
061282·22	35	27	19	0·060	0·88	0·012	4	0·152	1·11
070982·2	66	43	22	0·085	0·66	0·032	7	0·297	2·62
031983·11	55	30	5	0·241	2·17	0·060	43	0·322	2·94
031983·12	55	30	23	0·177	1·60	0·060	32	0·256	2·13
111583·1	68	43	27	0·077	0·58	0·047	9	0·311	2·80
052185·1	112	73	11	0·185	0·83	0·042	12	0·287	2·50
Mean (n = 7)	—	—	—	—	—	0·044	20	0·269	2·32

Columns (1)–(3) are as in Table 1. Column (4) gives the number of measurements of fibre absorbance at wave-lengths between 520 and 700 nm; column (5) the dye-related isotropic absorbance at 570 nm at the middle of the run; and column (6) the corresponding value of the dye concentration, $[D_t]$. Column (7) gives the best linear fit for the amplitude of the dichroic spectrum (A_0-A_{90}) by the isotropic spectrum $((A_0+2A_{90})/3)$; and column (8) the corresponding minimum concentration of oriented dye molecules required to explain column (7). Column (9) gives the fitted value for the fraction of the dye in the Mg^{2+}-bound form required to explain the shape of the isotropic spectrum, and column (10) the corresponding myoplasmic free $[Mg^{2+}]$ calculated by means of eqn. (10) in the text.

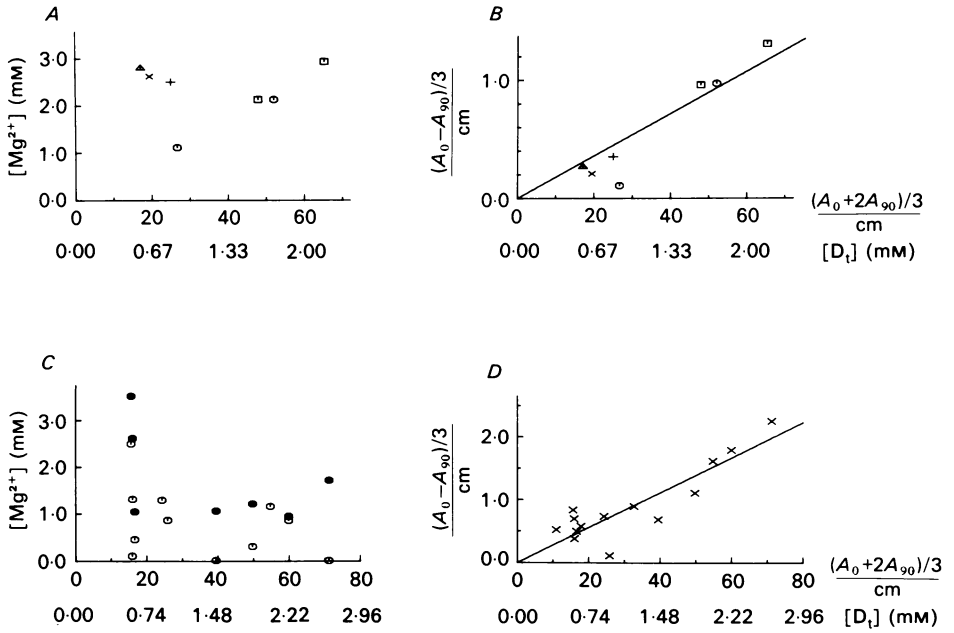

Fig. 5. Estimates of the myoplasmic free $[Mg^{2+}]$ (*A*, *C*) and the dichroic amplitude divided by three (*B*, *D*) as a function of the isotropic absorbance $(A_0+2A_{90})/3$ per cm path length, or equivalently, the average dye concentration, $[D_t]$, during the run. *A* and *B*, results with Arsenazo III; each experiment is identified by a different symbol. *C* and *D*, results with Antipyrylazo III. *C*, the open circles give the estimate of the $[Mg^{2+}]$ based on the uncorrected isotropic spectrum, whereas the filled circles give the estimate after correction for the spectral contribution from the bound and oriented molecules (see text). *B* and *D*, the best-fit straight lines through the origin have slopes of 0·018 and 0·028, respectively, corresponding to a minimum of 1·8 % and 2·8 % of the dye molecules being oriented in the 0 deg (fibre-axis) direction (see text).

wave-length). However, at 530 nm, where the earlier results (Baylor *et al.* 1982*a*) appear to have underestimated the contribution from the fibre intrinsic absorbance, the estimates differ significantly in the direction expected: 1·1 mM (±0·5 S.E. of mean) (Baylor *et al.* 1982*a*) and 3·6 mM (±0·4 S.E. of mean) (for the same seven runs from Table 2). Thus, the presumably more accurate method for removing the intrinsic absorbance described in this paper reveals the disturbing result that the $[Mg^{2+}]$ estimate obtained with Arsenazo III varies considerably as a function of wave-length. The validity of this conclusion is further supported by analysis of the runs in Table 2 at $\lambda = 600$ nm, where the average estimate of the $[Mg^{2+}]$ is 4·2 mM (±0·3 S.E. of mean). The fourfold difference between the $[Mg^{2+}]$ estimates at 600 nm and 650–660 nm was statistically highly significant ($P < 0.005$ Student's *t* test) and cannot be attributed to uncertainties in the intrinsic correction or in the assumed value of the internal pH (see calibrations in Baylor *et al.* 1982*a*; and Baylor *et al.* 1982*b*, Fig. 8). Rather, it is most likely to be due to spectral shifts attributable to bound dye molecules (see results with Antipyrylazo III described below). In the absence of a method for evaluating how dye binding may influence spectral shape,

the estimates of the free [Mg^{2+}] given in Table 2 have simply averaged the information over all wave-lengths ($520 \leqslant \lambda \leqslant 700$ nm) (see also Discussion).

Arsenazo III resting dichroism

In a previous study (Baylor *et al.* 1982*a*) a dichroic component to the resting spectrum of Arsenazo III in myoplasm was not detected. However, this result was based on data analysed at only one dye-related wave-length (570 nm) and obtained from fibres injected with generally small concentrations of dye (0·1–0·7 mM). Although indicating that Arsenazo III resting dichroism cannot be very large, these measurements did not rule out the possibility that a small resting dichroic signal might exist. In fact, the absence of dichroism in the resting spectrum might be unexpected in view of the detection of a prominent dichroic signal from Arsenazo III during fibre activity (Baylor *et al.* 1982*c*). The present set of experimental data were therefore examined carefully for the presence of a dichroic component in the Arsenazo III resting spectra. For the fibre of Fig. 3, which had the largest amount of injected dye, the result appeared convincing. Although small in amplitude, the muscle spectrum in Fig. 3*D*, which is proportional to the difference between the muscle spectra in Fig. 3*B*, was on average greater than zero. Moreover, its wave-length dependence was closely similar to that of the Arsenazo III isotropic spectrum (Fig. 3*C*), a finding in support of the interpretation that the dichroic signal was truly dye-related, and not an artifact of, for example, an improperly corrected intrinsic dichroic signal. When analysed by linear least-squares fitting (twenty-three absorbance measurements, including repeats, between 520 and 700 nm) the amplitude of the dichroic spectrum was 0·060 times the amplitude of the isotropic spectrum.

The results of this type of analysis applied to the seven spectral runs are summarized in Table 2, column (7). In all of the runs, the dichroic amplitude was a positive fraction of the isotropic amplitude. For the runs with smaller quantities of total dye ($[D_t] < 1{\cdot}0$ mM; see column (6) of Table 2) these numbers, considered individually, were not resolvably different from zero, due to the small amplitude of the dye-related dichroism and the necessity to correct for the intrinsic dichroism. However, averaged over the seven runs, the mean dichroic fraction, 0·444, was significantly different from zero ($P < 0{\cdot}02$, sign test). As discussed in Baylor *et al.* (1982*c*), this amount of dichroism could be explained by a sub-population of bound dye molecules, as little as 0·044/3, i.e. 1·5% of the total, whose absorbance moment was completely oriented along the fibre axis (0 deg direction). Alternatively, and undoubtedly more likely, a larger bound fraction might exist, for which the average orientation in the 0 deg direction is less complete. The minimum concentration of oriented molecules required to explain the observed dichroic signals is indicated in column (8) of Table 2 (see also Baylor *et al.* 1982*c*). In Fig. 5*B* the amplitude of the dichroic signal from the seven runs is plotted as a function of the amplitude of the isotropic signal. The data appear to be related in an approximately linear manner. The slope of the best-fit line in Fig. 5*B* corresponds to 1·8% of the total dye being bound and completely oriented along the fibre axis. This estimate of the mean fraction of oriented dye was also significantly greater than zero ($P < 0{\cdot}01$, linear regression analysis).

Although the estimated percentage of oriented Arsenazo III molecules is small

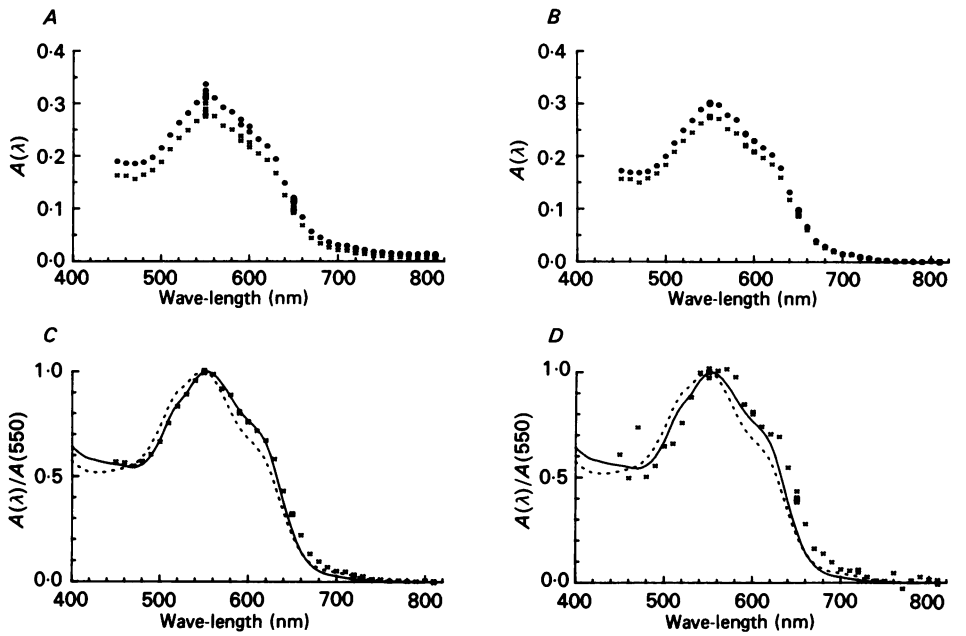

Fig. 6. Resting spectra from an Antipyrylazo III-injected fibre. *A*, absolute fibre absorbance (intrinsic + dye-related) measured with 0 deg (circles) and 90 deg (crosses) polarized light. *B*, dye-related polarized absorbances, A_0 (circles) and A_{90} (crosses), after subtraction of the intrinsic absorbance from the data in *A* and normalization for the steady decrease in dye concentration during the run (see text). *C*, isotropic dye absorbance (crosses) obtained from spectra in *B* as $(A_0+2A_{90})/3$ and scaled so that $A(550) = 1{\cdot}0$. *D*, dichroic dye absorbance (crosses), obtained from spectra in *B* as A_0-A_{90}. The curves in *C* and *D* are cuvette calibrations at a $[D_t]$ of 2·0 mM, pH 6·9, and a free $[Mg^{2+}]$ of 0 mM (continuous lines) or 1·61 mM (dashed lines). Fibre no., 031883·1; sarcomere spacing, 3·9 μm; average fibre diameter, 61 μm; spot diameter, 43 μm; 16·5 °C. The run was taken 60–76 min following injection. The average isotropic $A(550)$ of 0·28 corresponds to a $[D_t]$ of 2·6 mM.

(1·5–1·8 %), it should be emphasized that the estimate simply supplies a lower limit to the actual percentage of bound and oriented dye molecules. As is shown below in connexion with the Antipyrylazo III results, a slightly larger dichroic signal (2·8–3·0 %) can, by means of a spectral analysis, be associated with a much larger percentage (~34 %) of bound dye molecules.

General features of Antipyrylazo III absorbance in resting fibres

Measurements of polarized absorbance were made in a larger number of fibres injected with Antipyrylazo III than were injected with Arsenazo III and the results were analysed along the lines used for the Arsenazo III-injected fibres. Fig. 6 shows the results from a complete spectral run (λ = 450–810 nm in 10 nm steps) on a fibre injected with a large amount of dye, 2·6 mM (average value referred to the middle of the run). As for the spectra in Fig. 3, Fig. 6*A* shows the original absorbance measurements as a function of wave-length for the two forms of polarized light;

Fig. 6*B* shows the measurements after subtraction of the intrinsic fibre absorbance and normalization for the steady decrease in total dye concentration during the run; Fig. 6*C* shows the normalized isotropic spectrum, determined by averaging the measurements in Fig. 6*B* according to the weighting $(A_0 + 2A_{90})/3$; and Fig. 6*D* shows the normalized dichroic signal, which is proportional to $A_0 - A_{90}$. The curves in Fig. 6*C* and *D* are cuvette calibrations obtained with the free $[Mg^{2+}]$ at 0 and 1·6 mM. For purposes of comparison, these curves and the muscle data shown in Fig. 6*C* and *D* (crosses) were normalized to a value of 1·0 at $\lambda = 550$ nm, a wave-length which is an isosbestic point for the Mg^{2+}–Antipyrylazo III reaction (Appendix, Fig. 16).

It is apparent for the fibre of Fig. 6 that the isotropic spectrum of Antipyrylazo III in myoplasm is closely similar to that obtained in a calibrating solution at a free $[Mg^{2+}]$ of 0 mM. However, it is also clear from Fig. 6*B* that the 0 deg and 90 deg absorbance spectra have unequal amplitudes. The absolute difference in amplitudes (0·025 at $\lambda = 550$ nm) is much larger than can be reasonably attributed to uncertainties in the intrinsic correction. Thus, the existence of a dye-related dichroic signal is also indicated in the case of Antipyrylazo III. It is obviously a concern that the presence of the bound and oriented molecules underlying the dichroic signal might interfere with the determination of the free $[Mg^{2+}]$ from the shape of the isotropic spectrum. For example, the spectral shape of the dichroic component (Fig. 6*D*), although generally similar to that of the 0-Mg^{2+} calibration curve, on average appears to be more 'red-shifted' (translated to longer wave-lengths) with respect to the 0 mM-Mg^{2+} curve than does the isotropic spectrum. It should be noted that the Antipyrylazo III dichroic spectrum does not correspond to any realizable level of the free $[Mg^{2+}]$, as a red shift with respect to the 0 mM-Mg^{2+} curve would correspond to a 'negative' $[Mg^{2+}]$ (see below). It should also be noted that even the isotropic spectrum appears to be red-shifted with respect to the 0 mM-Mg^{2+} curve at long wave-lengths ($\lambda > 620$ nm), an effect which, while small, is apparently real (also see below).

The Antipyrylazo III resting isotropic signal

Under the assumption that errors introduced by the Antipyrylazo III dichroic signal are negligible, it is of interest to examine the shape of the isotropic spectrum as another indication of the free $[Mg^{2+}]$. The initial quantitative approach was analogous to that used for analysis of the Arsenazo III spectra, i.e. as given by eqns. (10) and (11), except that 550 nm was used as the isosbestic wave-length for the Mg^{2+}–dye reaction and 6·7 mM for $K_{D,Mg}$ (Rios & Schneider, 1981). Moreover, it was also desirable to extend the set of calibration spectra to deal with variations in $[D_t]$. This arises in the case of Antipyrylazo III because, as shown in the Appendix, the normalized shapes of the 0 mM-Mg^{2+} and $\Delta[Mg^{2+}]$ calibration spectra, where $\Delta[Mg^{2+}]$ is the change in the free $[Mg^{2+}]$, vary somewhat with $[D_t]$ in the range 0·4–2·0 mM. The reason for the dependence on $[D_t]$ is not known with certainty but is presumed to be due to the formation of dimers of dye not bound with Mg^{2+}. Whatever the exact explanation, the analogous least-squares fitting procedure may be carried out at the appropriate value of $[D_t]$ for each experiment to get the best description of the normalized muscle isotropic spectrum in terms of the 0 mM-Mg^{2+} and $\Delta[Mg^{2+}]$ cuvette spectra.

The results of this analysis are summarized in Table 3, columns (9)–(10), for eleven

TABLE 3. Analysis of Antipyrylazo III resting spectra for dichroism and the free $[Mg^{2+}]$

Fibre no. (1)	Fibre diameter (μm) (2)	Spot diameter (μm) (3)	No. of measurements (4)	$A(550)$ $(A_0+2A_{90})/3$ (5)	$[D_t]$ (mM) (6)	Fractional dichroic amplitude (7)	Oriented [dye] (μM) (8)	f_{Mg} (9)	$[Mg^{2+}]$ (mM) (10)	f^2_{Mg} (11)	$[Mg^{2+}]$ (mM) (12)
060882·1	54	30	23	0·0872	0·90	0·091	27	0·163	1·30	—	—
061082·21	104	57	22	0·3449	1·84	0·067	41	0·045	0·31	0·154	1·22
061082·22	96	57	10	0·1053	0·61	0·090	18	0·064	0·46	0·135	1·05
061582·1	81	43	14	0·0850	0·58	0·161	31	0·272	2·50	0·345	3·52
070282·1	64	43	12	0·1089	0·95	0·013	4	0·115	0·81	—	—
031883·1	61	43	37	0·2836	2·64	0·095	84	0·001	0·01	0·204	1·72
111583·2	65	43	12	0·0466	0·41	0·142	19	—	—	—	—
111683·1	69	43	19	0·1779	1·45	0·052	25	0·002	0·02	0·137	1·07
111783·1	50	30	34	0·0526	0·59	0·131	26	0·016	0·11	—	—
040384·2	97	57	17	0·1040	0·60	0·071	14	0·164	1·32	0·282	2·62
040784·21	112	73	7	0·2377	1·21	0·082	33	—	—	—	—
040784·22	112	73	7	0·1298	0·52	0·097	17	—	—	—	—
053084·21	81	57	6	0·3167	2·22	0·090	67	0·114	0·86	0·124	0·95
053084·22	81	57	12	0·2891	2·02	0·089	60	0·148	1·16	—	—
Mean	—	—	—	—		0·091 ($n=14$)	33 ($n=14$)	0·100 ($n=11$)	0·81 ($n=11$)	0·197 ($n=7$)	1·74 ($n=7$)

Columns (1)–(10) are analogous to those described in Table 2 except that for column (9) the wave-length range for the fitting was restricted to $520 \leqslant \lambda \leqslant 620$ nm. Columns (11) and (12) are corrected versions of columns (9) and (10) based on removal of the contribution due to the dichroic signal by the method described in the text. Where no figures are given in columns (9)–(12) runs were not fitted because of incomplete data.

f^2_{Mg} denotes the fraction of free molecules in the actual Mg^{2+}-bound form.

of the fourteen runs. Results were not analysed for three of the runs because the data were incomplete in the wave-length range 520–620 nm. This range of wave-lengths was selected for the fitting because the dye absorbance is most sensitive to the free $[Mg^{2+}]$ in this range and perhaps less likely to be influenced by other processes (see next section). On average, the results indicate that 0·10 of the total dye was bound with Mg^{2+} and that the myoplasmic free $[Mg^{2+}]$ was 0·8 mM. However, the estimates of the free $[Mg^{2+}]$ in the various runs showed considerable scatter, as is apparent in the plot of $[Mg^{2+}]$ *versus* $[D_t]$ (Fig. 5*C*, open circles). This variation was prominent even at a single value of $[D_t]$ (e.g. 0·6 mM) and over-all appeared to be larger than the corresponding variation in the estimates of $[Mg^{2+}]$ obtained from Arsenazo III using similar assumptions (Fig. 5*A*). One factor undoubtedly contributing to the greater variation is that the peak absorbance change for Antipyrylazo III per unit change in the free $[Mg^{2+}]$ is about 1·7 times less than the corresponding change for Arsenazo III (the peaks for both dyes occurring near 610–615 nm). Another, more important factor contributing to the more variable Antipyrylazo III results might be that the isotropic spectra measured from this dye are more heavily influenced by contributions from dye molecules that are not free in the myoplasmic solution.

The Antipyrylazo III resting dichroic signal

For each of the fourteen runs, the dye-related dichroic spectrum was computed and its fractional amplitude determined from a linear least-squares fit of the isotropic spectrum. The results of this analysis are summarized in columns (7) and (8) of Table 3. Column (7) shows that the fractional dichroic amplitude was in all cases a positive number, the value of which varied between 0·01 and 0·16. On average the fractional dichroic amplitude was 0·090, twice the comparable number for the Arsenazo III results. Moreover, as judged from the standard error of the measurements, this difference in the fractional dichroic amplitudes of the two dyes was statistically significant ($P < 0·01$, Student's *t* test). This difference is important as it argues strongly that the relatively small absolute amplitude of the orientation effect cannot be attributed to a methodological artifact. The Antipyrylazo III results indicate that, on average, a minimum of 0·090/3, i.e. 3·0 %, of the dye molecules were oriented at rest and presumably bound to oriented structures within the myoplasmic compartment. The minimal concentration of bound molecules required to explain the observed dichroic amplitude is given in column (8) of Table 3. Fig. 5*D* shows the amplitude of the dichroic signal as a function of the total dye concentration during each of the runs. The data are related in an approximately linear manner, with the slope of the best-fit line corresponding to a minimum of 2·8 % of the total dye molecules being oriented. As mentioned above for the Arsenazo III results, the presence of a larger fraction of bound dye molecules, correspondingly less well oriented along the fibre axis, may be considered a more likely explanation for the observed dichroic signal.

This quantitation of the dichroic amplitude has been made under the assumption that the underlying spectral components (isotropic and dichroic) are identical. While the close similarity of these two spectra (as seen, for example, in Fig. 6*C* and *D*) indicates that this assumption is quite reasonable for purposes of the estimates in Table 3, a quantitative examination of the two spectral shapes at wave-lengths

greater than 550 nm indicated a consistent difference. (Because of scatter in the measurements of the dichroic spectrum, it was not possible to determine if a consistent difference between isotropic and dichroic spectra also existed at wave-lengths less than 550 nm.) Table 4 provides a summary of this difference at $\lambda = 590$ nm and $\lambda = 650$ nm, the two wave-lengths greater than 550 nm where absorbance measurements were made most frequently. Column (3) and column (5) give the values of $A(590)/A(550)$ and $A(650)/A(550)$, respectively, for the dichroic signal in the nine runs for which the spectral amplitude was large enough for these numbers to be determined with reasonable accuracy. On average, the values were 0·86 ($\lambda = 590$ nm) and 0·42 ($\lambda = 650$ nm). For comparison, columns (4) and (6) give the same values determined for the thirteen isotropic spectra for which the measurement could be made. The isotropic values were on average smaller than the dichroic ones, being 0·76 ($\lambda = 590$ nm) and 0·25 ($\lambda = 650$ nm). Moreover, at 650 nm, the difference was statistically highly significant ($P < 0{\cdot}002$, sign test), as the entire range of measurements for the dichroic signal exceeded that of the isotropic signal.

A spectral estimate for the fraction of bound Antipyrylazo III molecules. Although the finding of an elevation in $A(\lambda)/A(550)$ for the dichroic compared with the isotropic spectra very likely holds at all wave-lengths greater than 550 nm, a quantitative estimate of this difference at 650 nm may be put to particular use. This situation arises because 650 nm is close to an isosbestic point for the Mg^{2+}–Antipyrylazo III reaction in the cuvette (Appendix, Fig. 16). Thus, the sub-population of dye molecules in the myoplasm for which the cuvette calibration conditions are appropriate should have a value of $A(650)/A(550)$ that is closely similar to the cuvette value, independent of the exact free $[Mg^{2+}]$ in myoplasm. As shown in the calibrations in the Appendix (Fig. 15*B*) and summarized in Table 4, column (7), the cuvette value of $A(650)/A(550)$ varies somewhat with $[D_t]$, e.g. between 0·18 and 0·24 for $[D_t]$ between 0·6 mM and 2·4 mM. However, as can be seen in column (10) of Table 4 (the difference between the data in columns (6) and (7)), the values of $A(650)/A(550)$ for the isotropic spectrum in myoplasm are consistently larger than expected on the basis of the cuvette estimates (all measured at a free $[Mg^{2+}]$ of 1·0 mM and referred to the corresponding values of $[D_t]$). One obvious explanation that may account for this difference is the contribution that the oriented molecules make to the isotropic spectrum. It therefore seemed of interest to pursue this explanation quantitatively under the assumption that there are two principal sub-populations of dye molecules: (i) a single bound and oriented population which directly gives rise to the measured dichroic spectrum; and (ii) the remaining molecules, which are presumed to be free in the myoplasmic solution and have a spectrum determined by the ionic conditions set by the cuvette calibrations at one of the levels of free Mg^{2+}. The difficulty in estimating the free $[Mg^{2+}]$ arises because the spectrum of this latter sub-population of dye molecules cannot be measured directly. However, under the above assumption, it follows that the measured isotropic spectrum, $A(\lambda)$, satisfies:

$$A(\lambda) = A_1(\lambda) + A_2(\lambda), \tag{12}$$

where $A_1(\lambda)$ is the absolute spectrum of the first sub-population and $A_2(\lambda)$ is the absolute spectrum of the remaining molecules. If the two underlying molecular

TABLE 4. Comparison of muscle isotropic and dichroic spectra and cuvette spectra for Antipyrylazo III

		Myoplasm				Cuvette					
Fibre no. (1)	$[D_t]$ (mM) (2)	Dichroic $\frac{A(590)}{A(550)}$ (3)	Isotropic $\frac{A(590)}{A(550)}$ (4)	Dichroic $\frac{A(650)}{A(550)}$ (5)	Isotropic $\frac{A(650)}{A(550)}$ (6)	'Initial' $\frac{A(650)}{A(550)}$ (7)	'Final' $\frac{A(650)}{A(550)}$ (8)	(5)−(7) (9)	(6)−(7) (10)	(10)÷(9) (11)	$\frac{(5)-(8)}{(6)-(8)}$ (12)
060882·1	0·90	—	0·690	—	0·206	0·198	—	—	0·009	—	—
061082·21	1·84	0·914	0·776	0·422	0·282	0·230	0·204	0·192	0·052	0·271	0·359
061082·22	0·61	1·015	0·759	0·445	0·244	0·183	0·177	0·262	0·061	0·233	0·250
061582·1	0·58	0·847	0·654	0·429	0·224	0·182	0·178	0·247	0·042	0·170	0·184
070282·1	0·95	—	0·756	—	0·205	0·198	—	—	0·007	—	—
031883·1	2·64	0·848	0·804	0·399	0·321	0·245	0·200	0·154	0·076	0·494	0·608
111583·2	0·41	—	0·871	—	0·212	0·172	—	—	0·040	—	—
111683·1	1·45	0·724	0·812	0·382	0·283	0·217	0·189	0·165	0·066	0·400	0·488
111783·1	0·59	—	0·815	—	0·205	0·182	—	—	0·023	—	—
040384·2	0·60	0·964	0·728	0·431	0·238	0·183	0·177	0·248	0·055	0·222	0·239
040784·21	1·21	0·846	0·764	0·408	0·280	0·209	0·187	0·199	0·071	0·357	0·421
040784·22	0·52	0·750	0·710	0·320	0·239	0·179	0·169	0·141	0·060	0·426	0·462
053084·21	2·22	0·863	0·739	0·540	0·245	0·237	0·234	0·303	0·008	0·026	0·037
Mean		0·863 ($n = 9$)	0·760 ($n = 13$)	0·419 ($n = 9$)	0·245 ($n = 13$)	—	—	—	—	0·288 ($n = 9$)	0·339 ($n = 9$)

Columns (3) and (4) give the ratio of the fibre absorbance at 590 nm to that at 550 nm for, respectively, the dichroic spectrum and the isotropic spectrum. Columns (5) and (6) give similar information for the spectra at 650 and 500 nm. Column (7) gives the ratio of the absorbance at 650 nm to that at 550 nm obtained in a cuvette at the myoplasmic dye concentrations given in column (2) and column (8) gives the ratio after correction for the estimated fraction of bound dye molecules given in column (12). As shown in the Appendix (Fig. 17*B*) the values in column (7) and column (8) depend slightly on the free $[Mg^{2+}]$; the numbers shown are for a $[Mg^{2+}]$ of 1 mM. Columns (9) and (1) give, respectively, the differences between columns (5) and (7), and columns (6) and (7). Column (11) gives the data in column (10) divided by that in column (9) and gives the 'initial' estimates of the fraction of bound dye. The data in column (12) were obtained in a manner analogous to those in column (11) but after the iteration procedure described in the text; column (12) therefore gives the 'final' estimate of the fraction of bound dye. Where no figures are given, this indicates that the data were too noisy to measure reliably. The data from fibre 053084·22 are not included, as $A(650)$ was not measured.

spectra $\epsilon_1(\lambda)$ and $\epsilon_2(\lambda)$ (in units of M^{-1} cm^{-1}) have an isosbestic point at a wave-length of 550 nm, then the normalized isotropic spectrum $A(\lambda)/A(550)$ satisfies:

$$\frac{A(\lambda)}{A(550)} = F_1 \frac{\epsilon_1(\lambda)}{\epsilon_1(550)} + (1-F_1) \frac{\epsilon_2(\lambda)}{\epsilon_2(550)}, \tag{13}$$

where F_1 is the fraction of total dye molecules that reside in the first sub-population. Since $\epsilon_1(\lambda)/\epsilon_1(550)$ is, by hypothesis, equal to the normalized dichroic spectrum, the normalized spectrum of $\epsilon_2(\lambda)/\epsilon_2(550)$, the shape of which is presumed to be set by the free $[Mg^{2+}]$, may be determined if an estimate of F_1 is available.

The analysis summarized in columns (7)–(12) of Table 4 was carried out in order to estimate the fraction F_1. The basis for making the estimate was to use eqn. (13) evaluated at 650 nm, a wave-length at which the dye absorbance is nearly independent of the free $[Mg^{2+}]$, and the data in columns (5) and (6) of Table 4 (available in their entirety for nine of the thirteen entries). For each fibre, the measured value of $A(650)/A(550)$ is given in column (6), the measured value of $\epsilon_1(650)/\epsilon_1(550)$ in column (5) and the (initial) estimate of $\epsilon_2(650)/\epsilon_2(550)$ in column (7). Therefore, column (11), which gives the ratio of the data in column (6) minus the data in column (7) to the data in column (5) minus the data in column (7), gives the (initial) estimate of F_1. The value in column (11) was a positive number in each run and was, on average, 0·29. This estimate of F_1, the fraction of $[D_t]$ that may be bound and oriented, is considerably larger than the lower limit of 0·03 determined from Table 3, column (7) or the regression line given in Fig. 5*D*. Moreover, the number is sufficiently large so as partially to invalidate the assumptions under which it was derived, namely, that the concentration of unbound dye appropriate for making the estimate of $\epsilon_2(650)/\epsilon_2(550)$ from Fig. 15*B* is the same as the $[D_t]$ given in column (2) of Table 4. In particular, since F_1 was significantly greater than zero in most experiments, the concentration of unbound dye was significantly less than the $[D_t]$. A correction for this effect requires the use of a smaller estimate of $\epsilon_2(650)/\epsilon_2(550)$ from Fig. 15*B*, which in turn increases the estimate of the bound fraction, which in turn reduces the amount of free dye, etc. However, after four or five iterations of this process, the estimation procedure converges to the 'final' values of $\epsilon_2(650)/\epsilon_2(550)$ given in column (8) of Table 4. The corresponding estimates of F_1 (i.e. after convergence) are given in column (12) of Table 4. The average value of the final estimates of F_1, the fraction of $[D_t]$ that is bound and oriented, was 0·34. It should be noted that although this analysis was carried out under the assumption that the dye molecules not in free solution belong to the oriented sub-population, F_1 may be interpreted more generally as the fraction of dye molecules having the same spectrum as the dichroic spectrum, independent of whether they are oriented or not (also see Discussion).

The analysis in Table 4 therefore supports the idea that: (i) a significant and possibly variable fraction of the total dye molecules in each experiment may not be free in the myoplasmic solution, and (ii) the resting spectrum of these dye molecules is significantly different from any cuvette calibration curve for $[Mg^{2+}]$. Taken together these effects would be expected to introduce significant errors in the estimate of the myoplasmic free $[Mg^{2+}]$ based on the measured shape of the isotropic spectrum alone, i.e. the approach used in the preceding section and summarized in Table 3, columns (9) and (10) and Fig. 5*C* (open circles).

A corrected estimate of the free [Mg^{2+}] *from Antipyrylazo III.* As a final step, corrected estimates of the myoplasmic free [Mg^{2+}] were made based on the estimate of the spectral shape $\epsilon_2(\lambda)/\epsilon_2(550)$ obtained by means of eqn. (13). For this analysis, the dichroic spectrum, $\epsilon_1(\lambda)/\epsilon_1(550)$ in the wave-length range $520 \leqslant \lambda \leqslant 620$ nm was assumed to have the shape of a cuvette calibration at some, possibly 'negative', level of free Mg^{2+}. The basis for this assumption can be seen in Fig. 6*D*, where the dichroic spectrum would appear to be well fitted by subtracting, and possibly scaling, the difference between the 1·6 mM-Mg^{2+} and 0 mM-Mg^{2+} calibration curves from the 0 mM-Mg^{2+} curve. It should be emphasized that the fitting of a 'negative' Mg^{2+} level has no physical significance, but is simply a mathematical convenience for describing the shape of the dichroic spectrum in the wave-length range $520 \leqslant \lambda \leqslant 620$ nm. Hence, by utilizing the relation in eqn. (11) (with 550 nm substituted for 570 nm) in combination with eqn. (13), it follows that:

$$\frac{\epsilon_0(\lambda)}{\epsilon_0(550)}+\frac{\Delta\epsilon_{max}(\lambda)}{\epsilon_0(550)}f_{Mg} = F_1\left(\frac{\epsilon_0(\lambda)}{\epsilon_0(550)}-\frac{\Delta\epsilon_{max}(\lambda)}{\epsilon_0(550)}f^1_{Mg}\right) + (1-F_1)\left(\frac{\epsilon_0(\lambda)}{\epsilon_0(550)}+\frac{\Delta\epsilon_{max}(\lambda)}{\epsilon_0(550)}f^2_{Mg}\right), \quad (14)$$

where f_{Mg} is the apparent fraction of all the molecules in the Mg^{2+}-bound form, f^1_{Mg} is the apparent fraction of the bound molecules having a spectral shape equivalent to a 'negative' Mg^{2+} spectrum, and f^2_{Mg} is the fraction of free molecules in the actual Mg^{2+}-bound form (the number which in combination with eqn. (10) allows the corrected estimate of the free [Mg^{2+}] to be obtained). This equation may be rearranged to give:

$$f^2_{Mg} = \frac{f_{Mg}+F_1 f^1_{Mg}}{1-F_1}. \quad (15)$$

Unfortunately, the shapes of the dichroic spectra were not sufficiently well determined in all experiments to allow an estimate of f^1_{Mg} to be made for each experiment. However, dichroic spectra from five of the runs were fairly well determined in the wave-length range, $520 \leqslant \lambda \leqslant 620$ nm. In each case the spectrum could be reasonably fitted by a Mg^{2+} calibration curve that was apparently 'negative'. The values so obtained for f^1_{Mg} were: 0·15, 0·15, 0·05, 0·13 and 0·21 (for runs using fibres 061082·21, 061082·22, 061582·1, 031883·1, and 040384·2, respectively). These values were used in eqn. (15) in combination with the values of F_1 estimated from the corresponding experiment (Table 4, column (12)) to obtain the corrected estimate, f^2_{Mg}, given in Table 3, column (11). In addition, there were two other analysable runs (fibres 111683·1, 053084·21), detailed in Table 3, for which F_1 could be estimated (Table 4); in these cases f^2_{Mg} was estimated from eqn. (15) by using the average value for f^1_{Mg} available from the other five runs, i.e. 0·14.

The values of f^2_{Mg} are presumed to reflect more accurately than f_{Mg} the free [Mg^{2+}] in the myoplasmic solution and were converted to the free [Mg^{2+}] (given in column (12) of Table 3) by means of eqn. (10), with $K_{D,Mg}$ assumed to be 6·7 mM. The average value for the seven runs was 1·7 mM (range 1·0–3·5 mM), a value more than twice that of the average of the uncorrected estimates given in column (10), Table 3. The corrected values from the individual runs are shown in Fig. 5*C* (filled circles).

Although the assumptions underlying the correction procedure are thought to be only roughly accurate, it is interesting to note that the correction reduced the scatter of the estimates somewhat and brought the average of the corrected estimates from Antipyrylazo III considerably closer to the average value of 2·3 mM estimated from the Arsenazo III measurements.

Azo1 absorbance in resting fibres

Measurements of absorbance spectra as a function of polarized light were also made on the fibres injected with Azo1. Since the spectrum of Azo1 in the cuvette is quite insensitive to levels of H^+ and Mg^{2+} in the physiological range (Tsien, 1983; Hollingworth & Baylor, 1986), no information concerning the concentrations of these ions in the myoplasm is available from this dye. However, its dissociation constant for Ca^{2+} ($K_{D,Ca}$) is quite low (3·7 μM at 20 °C) (Tsien, 1983; Hollingworth & Baylor, 1986) and therefore the resting dye absorbance spectrum might give information about the resting myoplasmic free [Ca^{2+}]. However, it should be noted that if the resting free [Ca^{2+}] is 0·1 μM or less, at most 2·6% (= 0·1/(0·1 + 3·7)) of the dye is expected to be in the Ca^{2+}-bound form. This will give a very small signal to measure reliably and set limits on. Secondly, although information concerning the possible degree of binding of the dye might be obtainable from the resting spectrum if resting dichroic signals were detected or if the isotropic spectrum were significantly shifted with respect to the cuvette calibrations, two factors have prevented the drawing of conclusive information on either of these points: (i) the main absorbance peak of the dye is positioned in the blue region of the spectrum, where the lower lamp intensities available from the tungsten–halogen bulb, particularly for wave-lengths less than 480 nm, introduce considerable uncertainty in the measurements, and (ii) the number of successfully completed experiments to date with dye concentrations large enough to measure Azo1 resting spectra reliably has been small. In spite of these difficulties, some information about Azo1 resting absorbance was obtained during seven spectral runs from five different fibres. Peak dye-related absorbances during the runs varied between 0·011 and 0·074 ($\lambda = 480$ nm). Under the assumption that $\epsilon(480) = 2{\cdot}57 \times 10^4$ M^{-1} cm^{-1}, i.e. that the dye was primarily in its Ca^{2+}-free form, this corresponds to dye concentrations between 0·1 and 0·5 mM.

An example of an Azo1 isotropic spectrum from myoplasm is shown in Fig. 7*A* (crosses); it is from the fibre injected with the largest concentration of dye (average value during the run was 0·5 mM). The spectrum has been corrected for the fibre intrinsic absorbance and for the steady decrease in $A(480)$ attributable to dye diffusion. In addition, the individual measurements of polarized absorbance have been averaged using the usual weighting, $(A_0 + 2A_{90})/3$. For comparison, the continuous curves in Fig. 7*A* show the spectra of Azo1 measured in cuvette calibrating solutions containing either no Ca^{2+} or saturating Ca^{2+} (Hollingworth & Baylor, 1986). The two curves have had the same relative scaling applied and reveal the expected isosbestic point at $\lambda = 404$ nm for the Ca^{2+}–dye reaction. It is clear from Fig. 7*A* that the muscle spectrum and the 0 mM-Ca^{2+} calibration curve have similar shapes when normalized by absorbance at $\lambda = 480$ nm. However, to estimate the fraction of dye in the Ca^{2+}-bound form in a resting fibre, it is important to have the spectrum

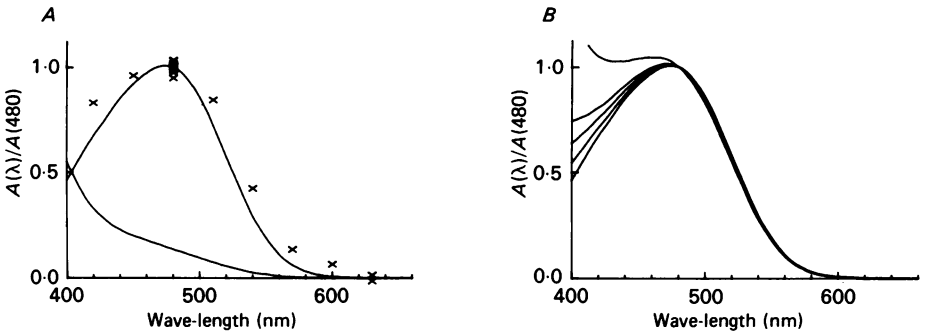

Fig. 7. Relative absorbance spectra of Azo1 in myoplasm and in cuvette. *A*, dye-related isotropic absorbance (crosses) from a fibre containing 0·5 mM-Azo1 normalized by the average value of $A(480)$ during the run of 0·074. Fibre no., 070184·1; sarcomere spacing, 3·6 μm; average fibre diameter, 87 μm; spot diameter, 57 μm; wide-band filters; 16 °C. The continuous curves are Azo1 spectra measured at 21 °C in a cuvette containing in mM: dye, 0·4; KCl, 140; HEDTA (*N*-hydroxyethylethylenediaminetriacetic acid), 11; and PIPES buffer, 10; pH 6·90. The curve that more closely fits the muscle data contained no added Ca^{2+}; the other curve contained 12 mM added Ca^{2+}, for which the effect on the absorbance change was saturating (not shown). Both curves were scaled by the same relative amount, namely, the factor which gave $A(480) = 1·0$ for the 0 mM-Ca^{2+} curve. *B*, cuvette calibration curves as in *A*, scaled in each case to give $A(480) = 1·0$. The curves were obtained at various levels of added Ca^{2+}, which were, in order of increasing relative absorbance at $A(400)$, 0, 1, 2, 3, and 6 mM, respectively, and which correspond to a free [Ca^{2+}] of 0, 0·6, 1·3, 2·2 and 6·9 μM, respectively. See text for additional details.

accurately measured and normalized at $\lambda = 404$ nm, the isosbestic point. Without this information, and in particular with only the data in Fig. 7*A*, no useful conclusion can be made about the fraction of Ca^{2+}-bound dye and therefore the free [Ca^{2+}]. This point is illustrated in Fig. 7*B*, where cuvette calibration curves obtained at various levels of free Ca^{2+}, 0, 0·6, 1·3, 2·2, and 6·9 μM, have been plotted after scaling to give a value of 1·0 at $\lambda = 480$ nm. The shapes of the curves for the various [Ca^{2+}] are all very similar at wave-lengths greater than 480 nm, the wave-length range where the muscle data are reliable. Thus the muscle data shown in Fig. 7*A* are equally consistent with any level of free Ca^{2+} up to several micromolar. However, because other measurements (Coray, Fry, Hess, McGuigan & Weingart, 1980; Blinks, Wier, Hess & Prendergast, 1982; Lopez, Alamo, Caputo, DiPolo & Vergara, 1983) indicate that the resting [Ca^{2+}] is 0·1 μM or less, it seems reasonable to assume that nearly all of the dye is in its Ca^{2+}-free form at rest.

(In Fig. 7, there is a strong suggestion that the muscle data (at $\lambda \geqslant 480$ nm) may, in fact, be red-shifted with respect to the cuvette calibration curves. Such a shift is not explained by the use of 30 nm (wide-band) filters in the muscle measurements compared with the very narrow band measurements made by the spectrophotometer. Unfortunately, there were not enough fibres that had been successfully injected with larger concentrations of Azo1 to decide if this apparent shift was a consistent pattern. However, two pieces of information suggest that the shift is real. In four of six spectral runs obtained on the other fibres, a similar, small shift was seen (see, for example, Fig. 8*B*). Over-all, however, the noise level in these other runs was such as to make

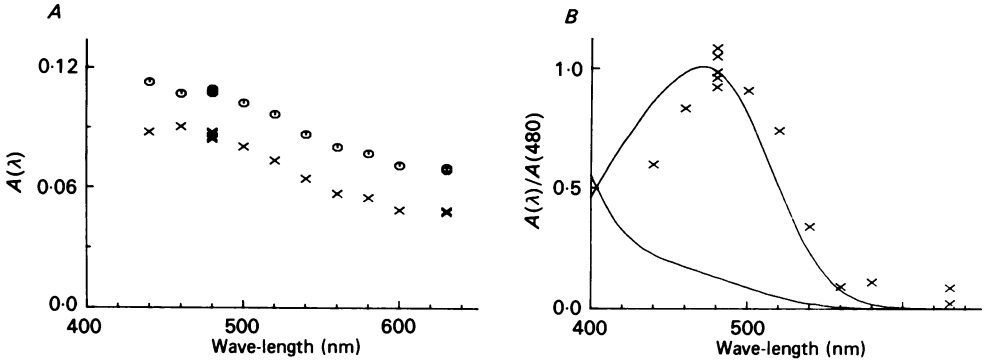

Fig. 8. *A*, total fibre absorbance (intrinsic+dye-related) in an Azo1-injected fibre measured with 0 deg (circles) and 90 deg (crosses) polarized light. Fibre no., 052485·1; sarcomere spacing, 4·2 μm; average fibre diameter, 110 μm; spot diameter, 73 μm; data taken 36–44 min after injection. *B*, dye-related absorbance (crosses) obtained from measurements in *A* after subtraction of intrinsic absorbance, normalization for dye diffusion and averaging of 0 deg and 90 deg signals. The data were scaled to a value of 1·0 for comparison with the cuvette calibrations (curves), which were the same as those in Fig. 7*A*. Before the scaling, the average value of $A(480)$ was 0·019.

the shift uncertain. Secondly, the spectrum of the Ca^{2+}-Azo1 signal detected during fibre activity appears to show a similar red-shift compared with the Ca^{2+}-Azo1 difference spectrum measured in cuvette calibrations (S. M. Baylor, S. Hollingworth, C. S. Hui & M. E. Quinta-Ferreira, unpublished observations). The latter shift in the active spectrum was more convincingly resolved than the resting spectral shifts mentioned here because of a greater resolution generally for measurements of active spectra. As concluded above in connexion with the Antipyrylazo III results, the presence of a red shift in the isotropic Azo1 spectrum is presumed to be indicative of a sub-population of Azo1 molecules that are bound within the myoplasmic space.)

Fig. 8 shows an example of absorbance spectra measured from a fibre injected with a much smaller concentration of Azo1, in which intrinsic absorbance was a large fraction of total fibre absorbance. Fig. 8*A* shows the raw measurements of fibre absorbance (intrinsic plus dye-related) as a function of 0 deg (circles) and 90 deg (crosses) polarized light. As expected for the intrinsic component alone, at long wave-lengths ($\lambda \geqslant 600$ nm), where the dye does not absorb, A_0 is greater than A_{90}. Fig. 8*B* shows the estimate of dye-related isotropic absorbance, obtained after correction for the intrinsic component and normalization for dye diffusion. As in Fig. 7*A*, the spectral shape is generally similar to a 0 mM-Ca^{2+} calibration curve (or any curve up to several micromolar Ca^{2+}). The peak value of absorbance at 480 nm, 0·019, corresponds to a $[D_t]$ of 0·1 mM. Fig. 8*B* illustrates that even in fibre locations containing 0·1 mM-dye or less, it is possible to make fairly accurate estimates of dye-related absorbance and therefore of $[D_t]$. Such estimates are particularly important for the calibrations of the free $\Delta[Ca^{2+}]$ measured with Azo1 during activity (Baylor *et al.* 1985; Hollingworth & Baylor, 1986) and have also been used to estimate the apparent diffusion constant of Azo1 in myoplasm (see next section).

(As for Arsenazo III and Antipyrylazo III, an attempt was made to evaluate from polarized absorbance measurements whether a detectable fraction of the Azo1 molecules were oriented. Based on the approach used for the other dyes (see Table 2, column (7) and Table 3, column (7)), the nominal amplitude of the Azo1 dichroic signal was estimated as a fraction of the isotropic signal. In all cases the fractional amplitude was small and not distinguishably different from zero. The accuracy of this statement is limited, however, due to the small dye concentrations and therefore small absolute absorbance levels. Nevertheless, it appears likely that if a fractional Azo1 dichroic signal as large as 0·1 existed, it would have been detected.)

Apparent diffusion constants of the dyes in the myoplasm

The above analyses of the wave-length and polarization characteristics of the dye spectra measured at any given fibre location and within a narrow window of time indicated the presence of at least two sub-populations of dye molecules in the case of both Arsenazo III and Antipyrylazo III. These include (i) the bound and oriented molecules, and (ii) the remaining, isotropically distributed molecules. In addition, it is likely that the isotropically distributed molecules themselves are not a homogeneous population, since molecules in the myoplasmic solution may be bound to other solution components, e.g. soluble proteins (Beeler *et al.* 1980). Another measurement that may give information about the fraction of dye molecules that are free within the myoplasmic solution is the dye's apparent diffusion constant in myoplasm, denoted D_{app}. For example, if most of the dye molecules are free, the work of Kushmerick & Podolsky (1969) suggests that D_{app} should be inversely correlated with the molecular weight of the dye and that it should be possible to predict D_{app} from their measurements of the diffusion constants of other molecules of somewhat smaller molecular weights. Since all three of the dyes have molecular weights of about 700 (776 for Arsenazo III, 746 for Antipyrylazo III, and 660 for Azo1), one would, in the absence of chemical restrictions to dye mobility (i.e. binding), expect to measure similar values for D_{app}, perhaps about $0{\cdot}8\text{–}0{\cdot}9 \times 10^{-6}$ cm^2 s^{-1} (estimate extrapolated from the data of Kushmerick & Podolsky, 1969, and referred to 16 °C assuming a Q_{10} of 1·3). Conversely, if the dyes have significant bound fractions, this might be detectable in terms of values of D_{app} significantly lower than $0{\cdot}8\text{–}0{\cdot}9 \times 10^{-6}$ cm^2 s^{-1} and, possibly, significantly different from each other.

Sufficient information for estimating D_{app} for the various dyes was available in a number of experiments, particularly in the case of Antipyrylazo III. The approach used for estimating D_{app} was similar to that employed by Blinks, Rudel & Taylor (1978), who estimated the distribution of aequorin in the myoplasm as a function of distance and time following injection of the protein at a 'point source' in the middle of the fibre. Analogously, in our dye-injected fibres, measurements of $[D_t]$ were estimated from the dye-related absorbance, $A(\lambda)$ (λ = 550 nm for Antipyrylazo III, 570 nm for Arsenazo III and 480 nm for Azo1). For each experiment the values were tabulated as a function of the distance x from the injection site and the time t after the injection. In all cases, the absorbance data were corrected as described previously for the fibre intrinsic absorbance measured at longer wave-lengths. In order to get the best estimate of D_{app}, the tabulated values of concentration, distance and time were

fitted under the assumption that dye distributes from the injection site according to the one-dimensional diffusion equation (Crank, 1956):

$$[D_t](x,t) = \frac{M}{2\sqrt{(\pi D_{app} t)}} \exp\left(\frac{-x^2}{4D_{app} t}\right), \quad (16)$$

where $[D_t]$, x and t are as defined above, M is the total amount of the substance per fibre cross-sectional area injected at $x = 0$ and $t = 0$ (μmoles cm^{-2}) and D_{app} is the apparent diffusion constant (cm^2 s^{-1}). For the fitting of any given data set, both D_{app} and M were adjusted so that the sum-of-squares deviation between observed and predicted values of $[D_t]$ was a minimum.

It should be noted that eqn. (16) is expected to apply if either (i) all the dye molecules are free to diffuse, in which case the actual diffusion constant, D, is the same as D_{app}, or (ii) there is a linear relation between bound (and immobilized) dye and free dye. In the latter case, D is related to D_{app} by:

$$D_{app} = \frac{D}{(1+R)}, \quad (17)$$

where R is the ratio of bound to free dye (see, for example, Crank, 1956, pp. 121–122).

An example of the procedure used for estimating D_{app} is shown in Fig. 9*A* for a fibre injected with Antipyrylazo III. The open circles show the measured values of $[D_t]$ as a function of distance from the injection site, which varied between -130 μm and $+770$ μm. It should be noted that the data were collected over a variable time period, 23–58 min after the injection. The fact that the data points correspond to different times as well as to different spatial locations does not complicate the fitting procedure *per se*, since each data point is equally weighted in the best fit according to its observed value minus that predicted by eqn. (16). The variable time interval does, however, mean that the theoretical fit cannot be plotted as a curve giving $[D_t]$ as a single-valued function of distance. For this reason, the theoretical fit is shown simply as the filled circles in Fig. 9*A*. (For the points in Fig. 9*A*, and in Fig. 9*B*, *C*, and *D*, in which there were more than one measured value at any given spatial location, the fitted values and the measured values changed progressively in the same order). Over-all, there was very good agreement between the observed and predicted data sets, with the best fit value of D_{app} being $0{\cdot}22 \times 10^{-6}$ cm^2 s^{-1}. A noticeably worse fit was obtained when D_{app} was changed by a factor of 1·3 in either direction.

Table 5 summarizes the results from the eight fibres injected with Antipyrylazo III for which sufficient spatial and temporal information was available to estimate D_{app}. The estimates fell within a reasonably narrow range, $0{\cdot}14$–$0{\cdot}29 \times 10^{-6}$ cm^2 s^{-1}, and had an average value of $0{\cdot}21$ ($\pm 0{\cdot}02$ S.E. of mean) $\times 10^{-6}$ cm^2 s^{-1}. It is of interest to note that this estimate, obtained at 16 °C in intact fibres, is somewhat lower than the value of $0{\cdot}36 \times 10^{-6}$ cm^2 s^{-1} estimated by Kovacs *et al.* (1983) for the longitudinal diffusion of Antipyrylazo III into cut frog fibres at 6–9 °C. However, our value from intact fibres is similar to the value of $0{\cdot}26 \times 10^{-6}$ cm^2 s^{-1} estimated by W. K. Chandler, M. Irving, J. Maylie & N. L. Sizto (personal communication) for the diffusion of Antipyrylazo III into cut fibres at 16 °C.

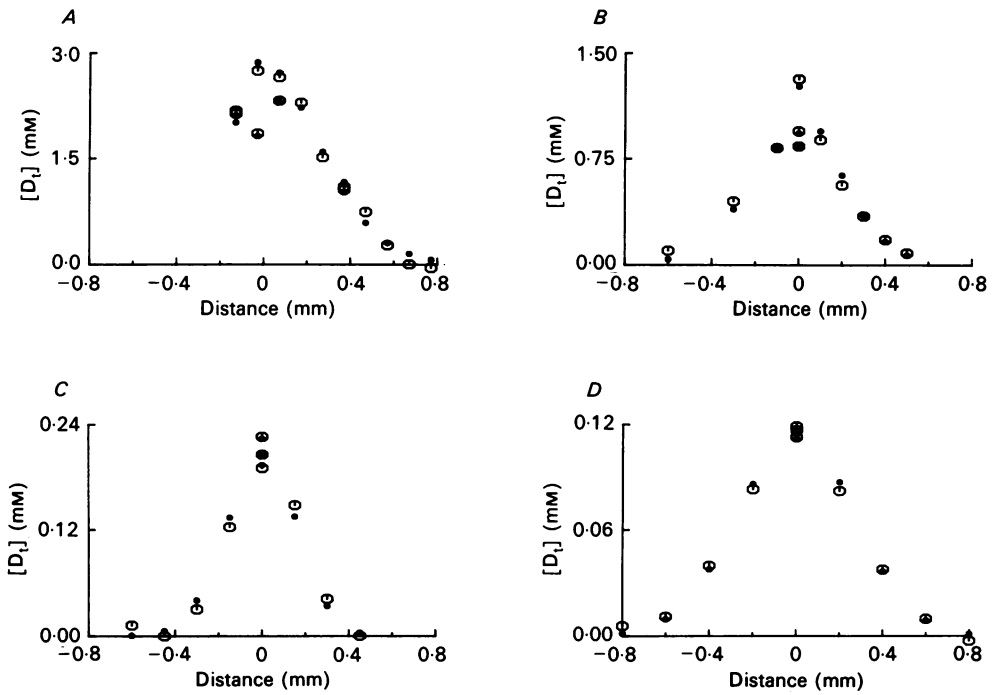

Fig. 9. Concentration of injected dye (ordinate) relative to axial distance from the injection site, in millimetres, along the fibre axis (abscissa). The measured concentrations (open circles) were estimated by Beer's law from the dye-related isotropic absorbance, whereas the calculated values (filled circles) are from the least-squares best fit of eqn. (16) after adjustment of M and D_{app}. (See Table 5 for the times of the measurements and the fitted values of M and D_{app}.) *A*, Antipyrylazo III; fibre no., 052184·1; sarcomere spacing, 3·4 μm; average fibre diameter, 63 μm; spot diameter, 43 μm; 17 °C. *B*, Arsenazo III; fibre no., 052185·1; sacromere spacing, 4·0 μm; average fibre diameter, 112 μm; spot diameter, 73 μm; 16 °C. *C*, Azo1; fibre no., 052485·1; sarcomere spacing, 3·8 μm; average fibre diameter, 115 μm; spot diameter, 73 μm; 16 °C. *D*, Fast Green FCF; fibre no., 052285·1; sarcomere spacing, 3·8 μm; average fibre diameter, 108 μm; spot diameter, 57 μm. Estimations of concentrations of Fast Green were based on the value of $\epsilon(620\text{ nm}) = 10{\cdot}9 \times 10^4\ \text{M}^{-1}\ \text{cm}^{-1}$ measured in a cuvette.

Fig. 9*B* shows analogous measurements of the dye concentration *versus* distance, and the corresponding theoretical fit to obtain D_{app}, in an Arsenazo III-injected fibre. The fitted value, $0{\cdot}10 \times 10^{-6}\ \text{cm}^2\ \text{s}^{-1}$, gave a very good description of the data, with a noticeably worse fit being obtained if D_{app} was changed by a factor of 1·3 in either direction. As indicated in Table 5, similar values were obtained in two other Arsenazo III experiments. The average value of D_{app} from the three experiments, $0{\cdot}12 \times 10^{-6}\ \text{cm}^2\ \text{s}^{-1}$, was somewhat lower than, but did not appear to be significantly different from, the average value of D_{app} obtained with Antipyrylazo III or the value of $0{\cdot}24 \times 10^{-6}\ \text{cm}^2\ \text{s}^{-1}$ measured for Arsenazo III at 16 °C in cut fibres by W. K. Chandler, M. Irving, J. Maylie & N. L. Sizto (personal communication). However, the number appears to be about 7–8 times lower than the value determined

TABLE 5. Apparent diffusion constants, D_{app}, for the dyes in the myoplasm

Fibre no. (1)	Sarcomere spacing (μm) (2)	Temperature (°C) (3)	Temporal variation (min) (4)	Spatial variation (μm) (5)	No. of measurements of $A(\lambda)$ (6)	Average $[D_t]$ at injection site (mM) (7)	M (μmoles cm^{-2}) (8)	D_{app} (10^{-6} cm^2 s^{-1}) (9)
Antipyrylazo III								
060382·1	3·9	16	10–24	+70, +270	13	2·1	0·11	0·24
061082·2	3·4–3·8	17	33–86	−500, +600	25	1·4	0·13	0·29
061582·1	3·6	16	58–99	−300, +50	10	0·4	0·05	0·25
031883·1	3·9	16	125–167	0, +1000	20	2·1	0·25	0·14
040784·2	3·4	17	44–99	+50, +675	13	0·7	0·07	0·23
052184·1	3·4	17	23–58	−130, +770	15	2·2	0·17	0·22
053084·2	3·3	16	100–124	−1050, +1050	17	1·9	0·19	0·14
060184·2	3·6	16	34–351	−410, +940	34	2·0	0·24	0·15
Mean (n = 8)								0·21
Arsenazo III								
061282·2	4·3	16	18–89	−350, 0	13	1·4	0·09	0·16
031983·1	4·4	16	27–89	−50, +280	5	1·2	0·09	0·10
052185·1	4·0	16	24–54	−600, +500	11	1·0	0·05	0·10
Mean (n = 3)								0·12
Azo1								
071084·1	3·8	16	9–81	+50, +580	7	0·4	0·03	0·18
110284·3	3·8	16	98–109	−500, +500	11	0·1	0·005	0·07
052385·1	4·0	16	22–50	−450, +450	18	0·1	0·005	0·09
052485·1	3·8	16	21–28	−600, +450	10	0·2	0·008	0·09
Mean (n = 4)								0·10
Fast Green FCF								
052285·1	3·8	16	71–78	−800, +800	11	0·1	0·008	0·08

Columns (4) and (5) give, respectively, the variation in time after the injection and the distance from the injection site for the individual measurements of dye-related absorbance. The number of such measurements during the run is indicated in column (6). The average concentration of dye at the injection site during the run is indicated in column (7). Columns (8) and (9) show the best fit of the parameters in eqn. (16) of the text.

for Arsenazo III by R. Rakowski (see personal communication quoted in Kovacs *et al.* 1983), who made the measurement on intact fibres microinjected with dye. The reason for the much higher D_{app} obtained by Rakowski is not clear.

Fig. 9*C* shows analogous results from an Azo1-injected fibre. The value estimated for D_{app} was $0{\cdot}09 \times 10^{-6}$ cm^2 s^{-1}, which was close to the average value of $0{\cdot}10 \times 10^{-6}$ cm^2 s^{-1} observed in four Azo1 experiments (Table 5). It should be noted, however, that the range of dye concentrations for the Azo1-injected fibres was considerably smaller than in most of the experiments with Arsenazo III or Antipyrylazo III, and the theoretical fits in the other Azo1 experiments had somewhat more noise. Over-all, however, the average value of D_{app} from the Azo1 experiments did not appear to be significantly different from the average values obtained with the other two metallochromic dyes.

Additional information about D_{app} in the myoplasm was obtained in a single experiment utilizing one other injected dye, Fast Green FCF (MW = 809). This dye, which is used in a variety of histochemical stains (Gurr, 1960), was one of several dyes selected for use in experiments marking the anatomical distribution of living neuronal cells, because of its ease of injection and ability to 'spread through the cytoplasm' (Stretton & Kravitz, 1973). Fig. 9*D* shows the measured longitudinal distribution of this dye 70–78 min after injection into a single fibre (open circles) as well as the theoretical best fit of the data by means of eqn. (16) (filled circles). The fitted value of D_{app}, $0{\cdot}08 \times 10^{-6}$ cm^2 s^{-1}, was slightly less than the average values of D_{app} measured with Azo1 and Arsenazo III.

Thus, the values of D_{app} measured for all four injected dyes were fourfold to tenfold lower than expected based on the extrapolated measurements of Kushmerick & Podolsky (1969) who used smaller sized molecules thought to be free within the myoplasmic solution. An obvious explanation for the reduced values of D_{app} is that large fractions of all the injected dyes are bound within the myoplasmic space, either to soluble components of larger molecular weight or to immobile structures accessible to the myoplasm.

Is D_{app} a function of $[D_t]$?

A question of interest that arises in connexion with the hypothesis that large fractions of the dyes are bound in the myoplasm is whether there is any correlation between D_{app} and $[D_t]$, or, equivalently, between D_{app} and the time after the injection when the measurement was made. For example, if the value of D_{app} is significantly influenced by dye binding, the effect of binding may be proportionately less at higher dye concentrations (or at earlier times after the injection). This might be revealed as a positive correlation between D_{app} and $[D_t]$, or a negative correlation between D_{app} and time, assuming that free dye diffuses more readily than bound dye. Fig. 10 shows the estimates of D_{app} from the eight Antipyrylazo III experiments, as a function of $[D_t]$ (Fig. 10*A*) and as a function of time after the injection (Fig. 10*B*). For these plots the results of each experiment are represented by a different symbol. For the population of fibres there appeared to be no correlation between the two variables in Fig. 10*A*, but a possible negative correlation between the variables in Fig. 10*B*. However, for two of the fibres (061082·2, 060184·2) sufficient data were available at significantly different times in the experiments to allow separate

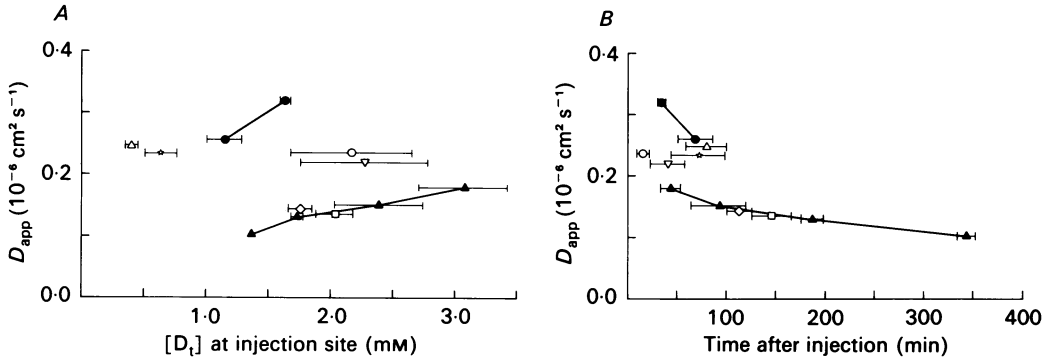

Fig. 10. Apparent diffusion constant, D_{app}, for Antipyrylazo III in the myoplasm as a function of: *A*, [D_t], the average dye concentration at the injection site at the mid-point of the run, as predicted from the theoretical fit of eqn. (16); *B*, the time following injection at which the measurements were made. A separate symbol has been used for each experiment. The two experiments for which more than one measurement of D_{app} were available are indicated by filled symbols (circles for fibre 061082·2; triangles for fibre 060184·2) and these measurements have been connected by line segments. The variation in predicted [D_t] (*A*) or time (*B*) during each run is indicated by the length of the horizontal bars.

estimates of D_{app} to be made at the different times. The data points for these two experiments have been plotted separately in Fig. 10 as filled symbols and connected with line segments. A sample of the original measurements obtained at the earliest and latest times from the experiment with four such runs (Fig. 10, filled triangles) is shown in Fig. 11. Considered individually, the fit for each of these runs was very good and appeared to be significantly better than the fits obtained if D_{app} was constrained to the average value of all the runs, $0{\cdot}15 \times 10^{-6}$ cm^2 s^{-1} (latter fits not shown in Fig. 11). Moreover, the fitted value of D_{app} changed progressively by a rather large fractional amount, whereas the four values of M estimated in the separate fits of the runs differed by only a few per cent, as expected for a constant total amount of injected dye. These data, while not conclusive, strongly suggest that within any given fibre there may be a positive correlation between D_{app} and [D_t] and a negative correlation between D_{app} and time, a suggestion that is lent additional support by the results from the second fibre (Fig. 10, filled circles). If correct, the correlated data from these two fibres provide further evidence in favour of the idea of significant dye binding in the myoplasm and, additionally, suggest that there is a non-linear relation between the [D_t] and the amount of bound dye.

Three other explanations may be proposed for the correlations between D_{app} and [D_t] and D_{app} and time in the two experiments above. First, the calculation of [D_t] from $A(550)$ assumed a constant extinction coefficient, $\epsilon(550)$, of $2{\cdot}7 \times 10^4$ M^{-1} cm^{-1}, although the measurements in Fig. 15*A* (Appendix) indicate that at low values of [D_t], $\epsilon(550)$ is larger than $2{\cdot}7 \times 10^4$ M^{-1} cm^{-1} whereas at high values the reverse is true. However, re-calculation of the values of D_{app} for the four runs on fibre 062184·2 based on the variable $\epsilon(550)$ given in Fig. 15*A*, yielded estimates of D_{app} that were in all cases reduced by a similar, small amount (4%). Thus, correction for a variable

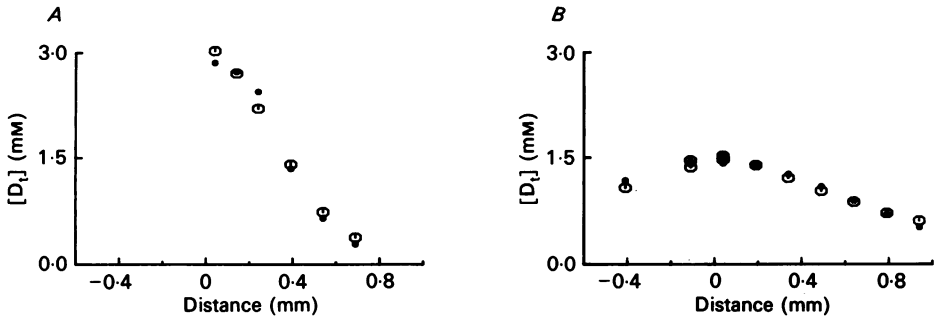

Fig. 11. Concentration of Antipyrylazo III (ordinate) relative to axial distance from the injection site (abscissa) at two different times in the same experiment. As in Fig. 9, the open circles are measurements made from dye-related isotropic absorbance ($\lambda = 550$ nm) and the filled circles show the fitted values based on adjustment of M and D_{app} in eqn. (16). Fibre no., 060184·2; sarcomere spacing, 3·6 μm; average fibre diameter, 63 μm; spot diameter, 43 μm; 16 °C. *A*, 34–54 min after injection: $M = 0{\cdot}245$ μmol cm^{-2}, $D_{app} = 0{\cdot}180 \times 10^{-6}$ cm^2 s^{-1}. *B*, 332–351 min after injection: $M = 0{\cdot}237$ μmol cm^{-2}, $D_{app} = 0{\cdot}105 \times 10^{-6}$ cm^2 s^{-1}.

extinction coefficient cannot explain the correlation. Moreover, it may also be noted that the direction of the correlation was opposite to that expected if dye dimerization (see Appendix) is important, since the amount of dye in the dimeric form, which may be presumed to have a smaller diffusion constant than the monomeric form, increases at higher $[D_t]$. Secondly, D_{app} was calculated under the assumption that dye was injected uniformly across an infinitely thin plane transverse to the fibre axis, whereas, in reality, a typical pressure injection introduced dye rapidly over some finite axial extent, usually some several tens of micrometres. However, re-analysis of the measurements under the assumption that the initial dye distribution was spatially homogeneous over a 50 μm length of fibre (rather than an infinitely thin extent) and that the appropriately integrated version of eqn. (16) was applicable, yielded estimates of D_{app} differing from the original estimates by less than 2%. Thus, an incorrect assumption about the initial shape of the dye profile would not appear to explain the correlation. Moreover, the direction of the correlation is opposite to that expected if radial as well as longitudinal diffusion of dye is important at early times after injection. In particular, the delay required for the movement of dye across the fibre at early times should lower rather than elevate the earliest measurement of D_{app}. A third possibility is that D_{app} might be correlated with $[D_t]$ and time coincidentally. For example, a correlation between $[D_t]$ and time might arise if there were some slow, time-dependent change in the myoplasm as a result of dye toxicity or damage secondary to the injection process. This possibility cannot be ruled out. However, the fibre of Fig. 11 was still functioning normally at the end of the experiment (6 h after injection), showed no visual evidence of an abnormal sarcomere structure along its length and had a nearly normal resting potential (−77 mV, measured with a micro-electrode in the dye-injected region).

While not considered experimentally conclusive, the correlation observed in Fig. 10 (filled symbols) was thought to be sufficiently suggestive to merit a quantita-

tive investigation in terms of dye binding. In particular, the specific shape of the correlation is presumed to contain information about the total concentration of binding sites for Antipyrylazo III and the binding constant of these sites for the dye. A computer model of longitudinal dye diffusion in combination with dye binding was therefore carried out for fibre 060184·2 under the following assumptions: (i) there is a binding of dye (Antipyrylazo III), of free and total concentrations [A] and [A_t], respectively, to a single population of sites, of free and total concentrations [S] and [S_t], respectively, which is characterized by a first-order dissociation constant, K; (ii) the kinetics of dye–site interaction are instantaneous with respect to diffusion time; and (iii) only the unbound dye is able to diffuse, for which an (actual) diffusion constant, denoted D, is applicable, independent of time and dye concentration.

As far as we are aware, there is no available analytical solution that gives $[A_t](x,t)$ under these assumptions. However, the dye diffusion process is presumably determined by the following system of equations, which may be simulated by computer:

$$[A_t](x,t+\Delta t) = [A_t](x,t) + D\frac{\partial^2[A](x,t)}{\partial x^2}\Delta t, \tag{18}$$

$$[S][A] = K[AS], \tag{19}$$

where Δt denotes a small increment of time and [AS] denotes the concentration of bound (and immobilized) dye and is equal to either $[A_t]-[A]$ or $[S_t]-[S]$. It is convenient to rewrite eqn. (19) as:

$$[A] = \frac{-(K+[S_t]-[A_t]) + \sqrt{\{(K+[S_t]-[A_t])^2 + 4K[A_t]\}}}{2}, \tag{20}$$

which may then be substituted into the right-hand side of eqn. (18) and thereby the shape of $[A_t](x)$ at time $t+\Delta t$ can be calculated from the shape of $[A_t](x)$ at time t.

In order to solve for $[A_t](x)$ at different times, a particular selection of the parameters D, $[S_t]$ and K must be made and the calculation initialized in some way. Moreover, a method for comparison with the experimental data must be chosen in order to decide how satisfactory was the particular selection of D, $[S_t]$ and K. The over-all procedure chosen was based on the empirical observation (see Fig. 11) that the dye profiles observed at the various times after injection were always well described by eqn. (16), the theoretical equation for one-dimensional diffusion in the absence of binding, or in the presence of linear (non-saturable) binding. The presumed effect of introducing the possibility of non-linear (saturable) binding, eqns. (18)–(20), is to account for decreases in D_{app} as a function of time, which otherwise should not take place. The data in Fig. 10*B*, fibre 060184·2, were therefore re-plotted (Fig. 12*A*) and the simulation initialized with respect to the earliest data point, i.e. by setting $[A_t](x)$ equal to the profile predicted by eqn. (16) at $t = 44$ min after injection if D_{app} was $0{\cdot}18 \times 10^{-6}$ cm^2 s^{-1} and M was 0·245 μmol cm^{-2} (see legend of Fig. 11). For each particular choice of D, $[S_t]$ and K, the profile was then either advanced or reversed in time according to whether Δt, applied to eqn. (18) was made positive or negative. At various times into the simulation, the dye profile was best fitted by eqn. (16) and the value of D_{app} plotted on the graph as a function of t. In all cases the fitted profiles gave a very good description of the simulated profiles.

This type of calculation was carried out under a number of parameter selections.

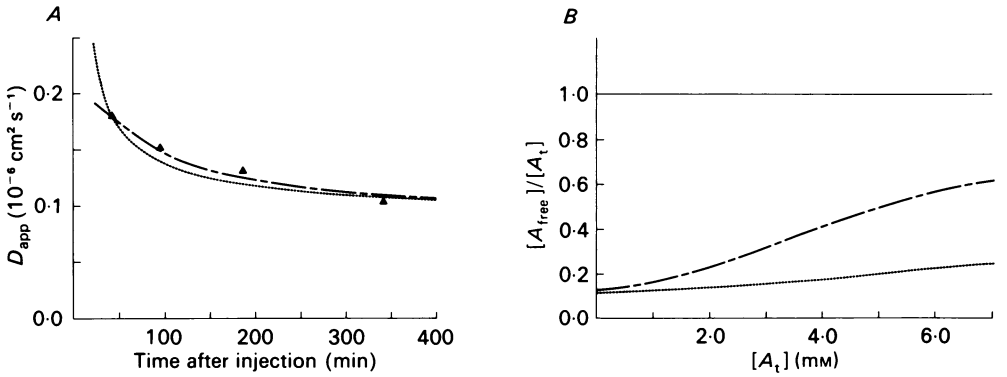

Fig. 12. Results of a computer simulation carried out for the purpose of explaining the decrease in D_{app} with time after injection observed in Fig. 10*B* for fibre 060184·2. For the simulation, longitudinal dye diffusion was assumed to obey eqns. (18)–(20) in the text, i.e. diffusion with saturable binding. *A*, the dotted curve was calculated assuming an actual diffusion constant D of $0{\cdot}60 \times 10^{-6}$ cm^2 s^{-1}, a total concentration of binding sites, $[S_t]$, of 9·0 mM, and a binding constant, K, of 1·20 mM; the dashed curve was calculated in the same way except with $D = 0{\cdot}30 \times 10^{-6}$ cm^2 s^{-1}, $[S_t] = 3{\cdot}0$ mM and $K = 0{\cdot}45$ mM. The computed values of D_{app} shown for the plot were obtained by fitting eqn. (16) to the simulated profile at the indicated time after injection (see text for details). *B*, plots of the ratio of freely diffusible dye, $[A_{free}]$, to total dye, $[A_t]$, calculated for the two sets of values assumed for D, $[S_t]$ and K in *A*. The horizontal line indicates the limiting case of 100 % of the dye in the freely diffusible state.

Results are shown in Fig. 12*A* for two parameter sets that gave reasonable fits to the data: (i) $D = 0{\cdot}60 \times 10^{-6}$ cm^2 s^{-1}, $[S_t] = 9{\cdot}0$ mM, K = 1·20 mM (dotted curve) and (ii) $D = 0{\cdot}30 \times 10^{-6}$ cm^2 s^{-1}, $[S_t] = 3{\cdot}0$ mM, $K = 0{\cdot}45$ mM (dashed curve). The dashed curve gives a somewhat better fit to the data points, whereas the dotted curve, which also gives an approximate fit, appears to describe better the suggestion from the population of results (Fig. 10*B*) that D_{app} may rise steeply as t approaches the time of injection. Over-all, the results shown in Fig. 12*A* indicate that the idea of diffusion with binding is a satisfactory explanation for the correlations noted in connexion with Fig. 10. However, the simulations also indicated that the measurements of D_{app} were not sufficiently well resolved to distinguish between these, and a number of other, parameter selections (not shown). In addition, the major assumption underlying the simulations, that there is a single population of binding sites, is undoubtedly an over-simplification. Nevertheless, as a final point, it was of interest to calculate the fraction of unbound dye molecules, $[A_{free}]/[A_t]$, as a function of $[A_t]$ for the two parameter selections simulated in Fig. 12*A*. These calculations are shown in Fig. 12*B* (dotted and dashed curves). These curves indicate that for either parameter selection a surprisingly small fraction of dye molecules are freely diffusible. For example, for the usual values of $[A_t]$ employed experimentally (< 3 mM), the calculated free fraction lies between 11 % and 32 %. Although these latter numbers are predicated on results from only one experiment, they also support the suggestion, made in connexion with Table 5, that a large fraction, possibly a majority, of the Antipyrylazo III molecules in the myoplasm may be bound.

DISCUSSION

Most experimental work to date on intracellular signals from metallochromic indicator dyes has reported measurements of changes in optical properties during cell activity using one or a few wave-lengths of unpolarized light. Relatively little attention has been paid to examination of the basic dye properties measurable in quiescent cells such as the spectral and polarization dependence of the signals or the diffusivity (apparent diffusion constant) of the dyes in the cytoplasm. In a general way, such measurements are important for testing the idea that the dye molecules reflect the ionic conditions of cytoplasm in a straightforward way. The experiments of this paper have extended the accuracy with which absorbance signals of this sort have been measured in intact single muscle fibres. The results obtained strongly suggest that assumptions routinely made in the analysis of intracellular dye signals may involve considerable error. For example, the measurements with all three metallochromic dyes employed in this study suggest that a major fraction of the dye molecules may be bound in the resting state, either to constituents of larger molecular weight dissolved in the myoplasmic solution or to oriented structures accessible to the myoplasm. This conclusion is consistent with that first reached by Beeler *et al.* (1980) who predicted from *in vitro* calibrations carried out in the presence of muscle components that 80–90 % of Arsenazo III at myoplasmic concentrations of 1–2 mM would be bound to soluble proteins (primarily) and other muscle constituents (secondarily). The conclusion is also consistent with the recent work of Irving *et al.* (1985) who, by studying the longitudinal diffusion of Antipyrylazo III into cut fibres, estimated that two-thirds of this dye is not freely diffusible.

Diffusion constants of the dyes in the myoplasm

The strongest evidence from the results of this paper that dye binding is a quantitatively large effect comes from measurements of the dyes' apparent diffusion constants, D_{app}. The average values of D_{app} fell in the range $0{\cdot}10$–$0{\cdot}21 \times 10^{-6}$ cm^2 s^{-1} for the three metallochromic dyes. These values for the myoplasmic diffusivity of molecules of molecular weight of about 700 are four- to ninefold smaller than extrapolated (see Results) from the data of Kushmerick & Podolsky (1969). According to eqn. (17), this suggests that three-quarters to eight-ninths of the dye molecules are bound to immobile sites. A quantitatively similar conclusion was reached based on results from a single Antipyrylazo III experiment analysed under somewhat different assumptions (see Fig. 12). In this fibre, D_{app} measured over a range of times after injection (44–342 min) was noted to decrease steadily with time, and the approximate time course of the decline could be accounted for in terms of a model which assumed diffusion with saturable binding. The estimated bound fraction varied somewhat as a function of the dye concentration, but the range of estimates for the dye concentrations used in most experiments (68–89 %, see Fig. 12*B*) is close to the range three-quarters to eight-ninths mentioned above. Moreover, since D_{app} for Azo1, one of the tetracarboxylate Ca^{2+} indicators (Tsien, 1980, 1983), was no larger than that found for the other dyes, Azo1 (and probably other tetracarboxylate dyes and buffers) may be presumed to have a similarly large bound fraction.

Polarization properties of the absorbance signals

The measurements of resting dye absorbance as a function of wave-length and polarization (Figs. 3–8) have also confirmed the existence of significant complexity attributable to dye binding. In the case of both Arsenazo III and Antipyrylazo III, polarized absorbance measurements indicated that detectable fractions of the dye molecules were preferentially oriented along the fibre axis, presumably because of binding to oriented structures accessible to the myoplasm, such as myofilaments or internal membranes. The orientation effect appeared to be significantly greater ($P < 0{\cdot}01$) for Antipyrylazo III than for Arsenazo III. Although the fraction of oriented dye molecules could conceivably be as small as 2–3 % (if the entire population of oriented molecules had their absorbance moment completely aligned along the fibre axis), a more likely situation is that the alignment is less complete and that the fraction of bound and oriented molecules is significantly larger. Such a situation is obviously consistent with the much larger bound fractions estimated from the dye diffusion constants (see previous section) or the somewhat larger fraction estimated from the isotropic and dichroic spectral curves (see next section).

Spectral properties of the absorbance signals

In the absence of dye binding, the isotropic absorbance spectra of the dyes should reflect the resting myoplasmic [Mg^{2+}] and [H^+] (in the case of Arsenazo III and Antipyrylazo III) or [Ca^{2+}] (in the case of Azo1). However, for Antipyrylazo III strong evidence was obtained that factors other than [Mg^{2+}] or [H^+] were important in determining the dye's spectral shape in the myoplasm. In particular, for wave-lengths greater than 620 nm, a red shift in the isotropic absorbance spectrum was detected that could not be attributed to any level of [Mg^{2+}] (Appendix) or [H^+] (Baylor *et al.* 1982*b*; S. Hollingworth & S. M. Baylor, unpublished observations). The red shift might conceivably be explained in terms of dye dimerization (see Fig. 13), but only if the dissociation constant for dimerization was significantly lower in the myoplasm than estimated from *in vitro* calibrations (see Fig. 14*B*). A more likely explanation, again, is that there is significant binding of dye to soluble or structural components and that the spectrum of the bound molecules is significantly red-shifted compared with that of the unbound molecules. This interpretation is supported by the finding that the spectrum of the oriented Antipyrylazo III molecules, which could be experimentally estimated, was red-shifted compared with the isotropic spectrum averaged over all the dye molecules or compared with any *in vitro* spectrum. From the amplitudes of the isotropic and dichroic spectra at 650 nm it was possible to estimate that perhaps one-third of the total Antipyrylazo III molecules in the myoplasm were bound. This estimate of the bound fraction might be either an over-estimate or an underestimate, depending on whether the average spectrum of all the bound molecules was, respectively, more or less red-shifted than that of the bound and oriented molecules. In particular, dye molecules bound to soluble (and therefore isotropically distributed) proteins would probably also have a red-shifted spectrum, but the average shift could be either more or less than that measured for the dichroic spectrum. The estimate of the bound fraction of the Antipyrylazo III molecules from the spectral information is thus not inconsistent with the larger

number estimated from the measurements of D_{app} or the smaller lower limit estimated from the measurements of polarized absorbance.

In the case of Arsenazo III, analysis of the isotropic spectrum also revealed an unexpected result, namely that the estimate of the free [Mg^{2+}] varied as a function of wave-length (3·6 mM at $\lambda = 530$ nm; 4·2 mM at $\lambda = 600$ nm; 1·0 mM at $\lambda = 650$–660 nm). Such variation should not arise unless bound molecules exist in appreciable quantity and have a spectral shape significantly different from that of free dye molecules (either associated or unassociated with Mg^{2+}). Unfortunately, since no reliable information was available about the spectral shape of the bound Arsenazo III molecules, no quantitative estimate concerning the fraction of bound dye molecules could be made from the spectral and polarization information alone.

In one clearly resolved experiment with Azo1 at a myoplasmic concentration of 0·5 mM, the resting spectrum of Azo1 (for $\lambda \geqslant 480$ nm) appeared to be red-shifted compared with any cuvette calibration for [Ca^{2+}]. Such a shift is consistent with the inferences from D_{app} about the existence of a large bound fraction for Azo1 and the red-shifting effect that binding was observed to have on the Antipyrylazo III spectra.

The practical significance of differences between the various methods for detecting bound dye

In the case of all three dyes, the presence of small dichroic components or of small, unexplained shifts in the isotropic spectra appear, as judged from measurements of the dye diffusion constants, to be correlated with the existence of large fractions of bound dye. This correlation may be of interest to investigators using indicator dyes in other cells where spectral or polarization information from the dye molecules may be more readily obtainable than accurate measurements of dye diffusion constants. Since large fractions of bound dye might result in important interference in the measurement of the ionic species of interest, it would appear that unexpected polarization and spectral effects seen with indicator dyes, even if small, should not be dismissed lightly.

Revised estimates of the myoplasmic free [Mg^{2+}] based on metallochromic dye signals

A number of reports are now available in the literature in which the myoplasmic free [Mg^{2+}] has been estimated by means of metallochromic dyes injected into intact frog skeletal muscle fibres. The estimates vary over a wide range, both for results based on the use of a single dye in more than one laboratory, and for results based on the use of more than one dye in a single laboratory. For example, estimates using Arsenazo III range from 0·5 mM ($500 \leqslant \lambda \leqslant 700$ nm, assumed internal pH = 7·1; Miledi *et al.* 1982), to 1·2 mM ($\lambda = 530$ and 650 nm, assumed internal pH = 6·9; Baylor *et al.* 1982*a*), to 2·3 mM ($520 \leqslant \lambda \leqslant 700$ nm, assumed internal pH = 6·9; this paper), to 3·5 mM ($\lambda = 600$ nm, assumed internal pH = 7·1; Close & Lannergren, 1984). In addition, Baylor *et al.* (1982*a*) estimated a level of 0·3 mM using Dichlorophosphonazo III and 6·0 mM using Arsenazo I (assumed internal pH = 6·9 in both cases). To these numbers may now be added the estimates in this paper from use of Antipyrylazo III, namely 0·8 mM if uncorrected for the effects of bound dye, or 1·7 mM if corrected for the effects of bound dye under the assumptions stated in the Results ($520 \leqslant \lambda \leqslant 620$ nm, assumed internal pH = 6·9).

The variability arising in the use of Arsenazo III in different laboratories does not appear to be attributable to the methods chosen for the *in vitro* calibrations of the Mg^{2+}–Arsenazo III reaction. Rather, it is presumably due to the method chosen for subtracting the intrinsic fibre absorbance in combination with the choice of the particular wave-lengths, or wave-length ranges, used for making the estimates of the myoplasmic dye absorbance. A detailed justification is given in the Results for the choice of the particular methods used in this paper and, in terms of the absorbance measurements *per se*, they are thought to be more accurate than methods previously employed on intact fibres. Nevertheless, the use of these methods has not reconciled the variability in the (uncorrected) estimates based on the use of more than one dye, or even of one dye (Arsenazo III) when the estimates are analysed as a function of wave-length.

An explanation for such variability was proposed by Baylor *et al.* (1982*a*) and is lent additional support by the measurements in this paper, namely, the effects of dye binding to intracellular constituents. If indeed large fractions of the dye molecules are bound, there is no reason to suppose that accurate estimates of ionic levels can be made from the spectral properties averaged over all the dye molecules. One can imagine certain specialized circumstances in which dye binding might introduce relatively little error, for example, if (i) the bound dye had the same affinity for Mg^{2+} as well as the same spectral properties as the unbound dye, or (ii) the bound dye was insensitive to Mg^{2+} but fortuitously had the same absorbance at a particular wave-length as the free dye at the usual myoplasmic free $[Mg^{2+}]$. However, such circumstances appear not to be the case in general and there is an obvious need for experimental characterization of the effects of dye binding, e.g. by means of *in vitro* calibrations involving muscle components (see Beeler *et al.* 1980), before *in vivo* measurements observed with any particular dye can be claimed to be properly analysed. Since, to date, myoplasmic $[Mg^{2+}]$ calibrations have not taken into account the properties of bound dye, it is perhaps not surprising that a wide range of inconsistent results have been obtained.

Nevertheless, a cautiously optimistic interpretation of the results obtained here with Arsenazo III and Antipyrylazo III may be worth proposing, since the polarized absorbance measurements made with Antipyrylazo III have allowed at least a partial characterization of the spectral effects of dye binding. For this dye, a quantitative comparison of the isotropic and dichroic spectra with each other and with spectra from cuvette calibrations was made. From the estimate that, on average, one-third of the dye molecules in myoplasm were bound and had a red-shifted spectral shape, it was concluded that the average free $[Mg^{2+}]$ indicated by the remaining dye molecules was 1·7 mM, a level substantially higher than the 0·8 mM estimated from the spectral contributions of all the dye molecules. A similar sort of correction applied to the Arsenazo III estimate averaged over all wave-lengths would undoubtedly also be appropriate, since evidence for a bound fraction of Arsenazo III molecules was also obtained from the measurements of spectral shape, polarized absorbance and the apparent diffusion constant of the dye. Unfortunately, it was not possible to use the Arsenazo III dichroic signal to make a quantitative correction for the spectral effects of bound dye, since the Arsenazo III dichroic signal was small in amplitude and its spectral shape not well resolved. However, it is interesting to note that an uncorrected

red shift due to bound Arsenazo III molecules might be expected erroneously to increase the indicated free [Mg^{2+}] since a red shift in the case of this dye would appear as a positive Mg^{2+} level (see Fig. 3*C*) as opposed to the negative level seen with Antipyrylazo III (see Fig. 6*C*, $520 \leqslant \lambda \leqslant 620$ nm). Thus, a correction for bound and red-shifted Arsenazo III molecules would presumably reduce the estimate of the [Mg^{2+}] obtained from the average of all the dye molecules, possibly to a level close to that of the corrected Antipyrylazo III estimate. In other words, since the uncorrected estimates obtained with Arsenazo III and Antipyrylazo III may represent upper and lower limits, respectively, there is some basis for concluding (even without having available an estimate correcting for bound Antipyrylazo III) that the free [Mg^{2+}] may lie in the range 1–2 mM (assumed internal pH = 6·9). Whether polarized absorbance measurements with Dichlorophosphonazo III and Arsenazo I might be reconciled with an estimate in the low millimolar range is a question that requires further experimental investigation.

APPENDIX

This Appendix contains information about the absorbance spectra of Antipyrylazo III measured in cuvette calibrations as a function of the [D_t] and free [Mg^{2+}]. This information forms the basis for the interpretation of the Antipyrylazo III spectra measured from the myoplasm in resting muscle fibres and described in the body of the paper.

The *in vitro* dye absorbance spectra were measured as described previously (Hollingworth & Baylor, 1986) on a U.V./visible spectrophotometer (Model 4050, LKB Instruments Incorporated). The standard calibrating solution contained in mM: KCl, 140; EGTA (ethyleneglycol-bis(β-aminoethylether)*N*,*N*′-tetraacetic acid), 1; K_2PIPES, 10, titrated to pH 6·90 with KOH. To this solution various additional amounts of Mg^{2+} were added (as $MgCl_2$) as well as various amounts of dye. Following the additions, the pH of all solutions was re-measured and, where necessary, re-titrated to pH 6·90. Due to heat emitted by the spectrophotometer, the temperature of the measurement compartment of the instrument was some 10 °C above the ambient temperature when at a steady state. The calibrations were therefore carried out after placing the spectrophotometer in a refrigerator, where the temperature in the measurement compartment was monitored by a thermistor and kept at 20 °C (±1 °C). Dye absorbances were usually measured in 5 nm increments between 400 and 800 nm.

The first complication that arose in the interpretation of the absolute spectrum of Antipyrylazo III was that its shape in a 0 mM-Mg^{2+}/0 mM-Ca^{2+} solution was not independent of the [D_t]. This effect is illustrated in Fig. 13. Fig. 13*A* shows absolute spectra obtained at three different values of [D_t], 0·016 mM (continuous curve, measured in a 1 cm cuvette), 0·8 mM (dashed curve, measured in a 0·05 cm cuvette) and 2·0 mM (dotted curve, measured in a 0·05 cm cuvette). The values of [D_t] were estimated by weight of the anhydrous dye, under the assumption that the Antipyrylazo III salt supplied by ICN K and K Labs (Plainview, NY, U.S.A.) had a molecular weight of 792. For purposes of comparison, the curves in Fig. 13*A* have had a relative scaling applied, equal in all cases to $([D_t] \times l)^{-1}$, where l is the cuvette

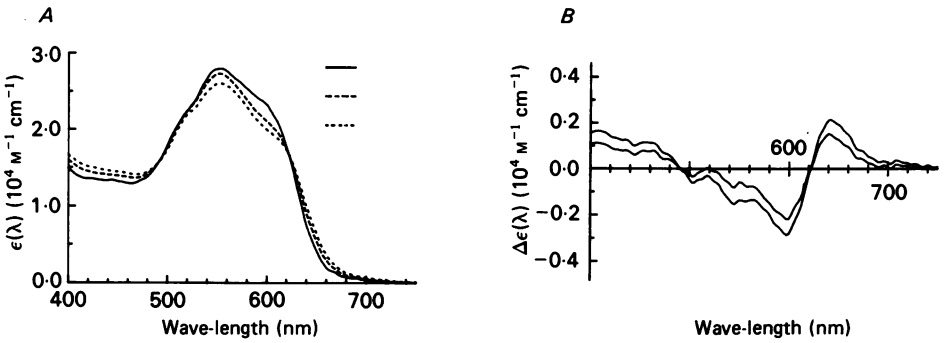

Fig. 13. Spectrophotometer calibration spectra of Antipyrylazo III at three different values of $[D_t]$ in a solution containing in mM: KCl, 140; K_2PIPES, 10; EGTA, 1; (pH 6·90, 20 °C, no added divalent ions). The ordinate in *A* and *B* is in molar extinction units (10^4 M^{-1} cm^{-1}), which is obtained by dividing the raw spectra by the product of the $[D_t]$ and the path length. *A*, continuous curve, $[D_t]$ = 0·016 mM, measured in a 1 cm cuvette; dashed curve, $[D_t]$ = 0·8 mM, measured in a 0·05 cm cuvette; dotted curve, $[D_t]$ = 2·0 mM, measured in a 0·05 cm cuvette. *B*, difference spectra obtained from *A* by subtracting the continuous curve from the dashed and dotted curves. If all dye molecules existed in a single state (e.g. were monomeric), the difference spectra in *B* would be flat.

path length. Thus the curves are displayed in units of molar extinction coefficient (M^{-1} cm^{-1}), which allows for a direct comparison of the molecular spectra of the dye. It is clear that the spectra in Fig. 13*A* do not superimpose. At short wave-lengths (λ < 490 nm) or at long wave-lengths (λ > 620 nm), the 2·0 mM curve is above the 0·016 mM curve, whereas at intermediate wave-lengths the reverse is true. A qualitatively similar effect is seen in the case of the 0·8 mM curve, which lies between the 0·016 and 2·0 mM curves throughout the wave-length range. The fact that the curves do not superimpose indicates that Antipyrylazo III molecules in the basic calibrating solution free of divalent ions coexist in more than a single state. Some interaction as a function of the $[D_t]$ is indicated, most likely the formation of a higher order dye complex. In this regard it is interesting to note that the principal complex that Antipyrylazo III forms in the presence of low levels of Ca^{2+} is a dimeric one, one Ca^{2+} plus two dye molecules (Rios & Schneider, 1981). The possibility that the effect in Fig. 13*A* is due to Ca^{2+} can, however, be ruled out since the free $[Ca^{2+}]$ must have been negligibly small in all solutions, which contained 1 mM-EGTA and no added Ca^{2+}.

The nature of the interaction giving rise to the effect can be examined more directly by subtracting the spectrum measured at the low dye concentration (0·016 mM) from the spectra measured at the higher dye concentrations. Examples of two such 'differences' spectra, $\Delta\epsilon(\lambda)$, are shown in Fig. 13*B* at higher vertical gain. The difference spectra have very similar shapes, characterized by an absorbance increase at the very long or very short wave-lengths, two isosbestic points (near 490 and 620 nm) and a multi-peaked decrease in absorbance between 490 and 620 nm. The fact that the spectral shapes are similar indicates that the formation of a single higher order complex, in addition to free dye, may be sufficient to explain the effect shown in Fig. 13*A*. It is also apparent that at higher $[D_t]$ more of the higher order complex is formed.

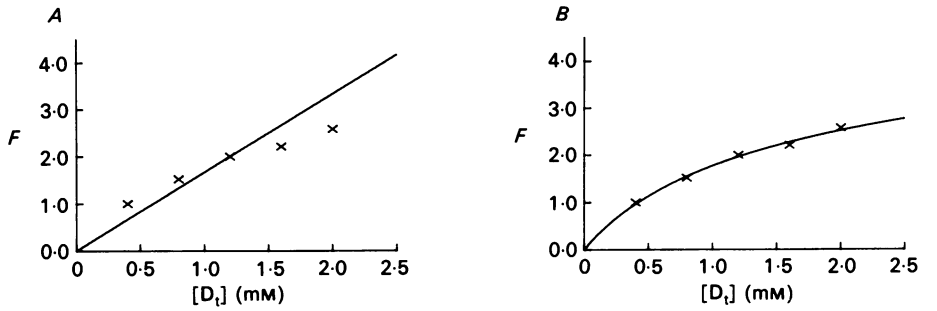

Fig. 14. F values (crosses) as a function of $[D_t]$. The F value is the least-squares linear scaling factor of difference spectra obtained as in Fig. 13B fitted by the smallest such difference spectrum, namely, the difference between the absolute spectrum obtained at a $[D_t]$ of 0·4 mM and that obtained at a $[D_t]$ of 0·016 mM. (The latter point, by definition, corresponds to $F = 1{\cdot}0$ at $[D_t] = 0{\cdot}4$ mM.) The curve in A is a fit by eye of a straight line intersecting the origin. The curve in B is the least-squares best fit of the theoretical shape expected if the effect in Fig. 13 is explained by dye dimerization. The fitted value of the dissociation constant was 4·0 mM (see eqn. A 2 and text for details).

Fig. 14A (crosses) shows the amplitude of difference spectra of the type shown in Fig. 13B as a function of $[D_t]$. Although there is some scatter associated with the measurements, the data lie near a line which intersects the abscisssa at a $[D_t]$ of 0·016 mM. A relation of this kind is expected if the higher order complex is a dimer. In this case, according to the law of mass action, the concentration of monomers, [D], would be related to the concentration of dimers, $[D_2]$, by:

$$K[D_2] = [D]^2, \tag{A 1}$$

where K is the dissociation constant for the reaction. The fraction of the total dye molecules in the dimer form, f_2, would then satisfy:

$$f_2 \equiv \frac{2[D_2]}{[D_t]} = \frac{[D]}{[D]+K/2}. \tag{A 2}$$

Moreover, if the range of the $[D_t]$ is small with respect to $K/2$, f_2 will be a small fraction and approximately satisfy:

$$f_2 \approx \frac{[D_t]}{K/2}. \tag{A 3}$$

Since, under the dimer hypothesis, difference spectra of the type shown in Fig. 13B are proportional to f_2, the plot in Fig. 14A is expected to be linear. These considerations, while not ruling out more complicated hypotheses, indicate that the effect apparent in Fig. 13 is roughly consistent with dye dimerization.

The data in Fig. 14A do, however, show a systematic deviation from the straight line fit, being above the line at lower $[D_t]$ and below the line at higher $[D_t]$. A deviation in this direction is expected if f_2 is not always a small fraction of the $[D_t]$ in the range employed for the measurements. In this case, [D] may be significantly smaller than $[D_t]$ and the effects of partial saturation need to be taken into account. The data have therefore been replotted (Fig. 14B) after a least-squares fit obtained by adjusting two

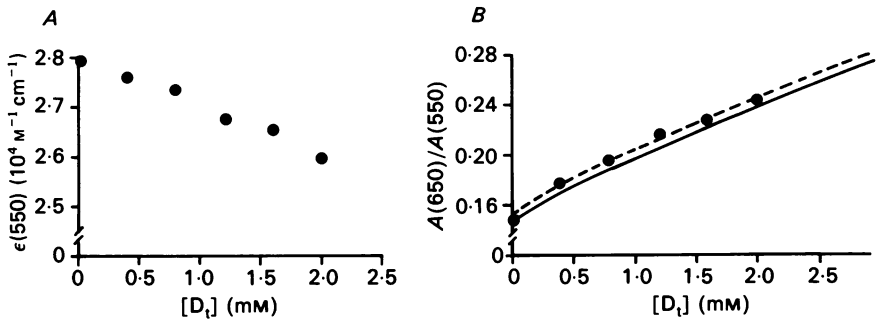

Fig. 15. *A*, molar extinction coefficients (filled circles) of Antipyrylazo III at 550 nm, $\epsilon(550)$, as a function of $[D_t]$, measured from curves as in Fig. 13*A*. *B*, absorbance ratios (filled circles), $A(650)/A(550)$, as a function of $[D_t]$, measured from curves as in Fig. 13*A*, i.e. at a free $[Mg^{2+}]$ of 0 mM. The dashed curve has been fitted by eye. The continuous line is a similarly generated curve but appropriate to a free $[Mg^{2+}]$ of 1·0 mM, obtained by interpolation between measurements obtained in solutions containing total $[Mg^{2+}]$ of 1·0 and 2·0 mM (see text).

parameters: the value of K in eqn. (A 2) and the maximum extinction change, $\Delta\epsilon_{max}(\lambda)$, expected when all the dye is in the (hypothetical) dimeric form. With the extra parameters, a much better fit of the theory to the data is found. The fitted values are $K = 4{\cdot}0$ mM and a peak $\Delta\epsilon_{max}(\lambda)$ of $-0{\cdot}88 \times 10^4$ M^{-1} cm^{-1} occurring at $\lambda = 598$ nm ($\Delta\epsilon$ referred to a single dye molecule). Similar spectra and fitted values were obtained in a second series of measurements (not shown). However, it should be noted that the range of $[D_t]$ employed for the measurements in Fig. 14*B* was evidently not large enough to force a major fraction of the dye into the dimeric form (and significantly larger values of $[D_t]$ could not be used without the dye slowly beginning to precipitate). Thus, the saturating level, $\Delta\epsilon_{max}$, and hence also K, are subject to some uncertainty. The results obtained from the best fit, however, suggest that a significant fraction of the dye is not in its monomeric form at values of $[D_t]$ typically used for intracellular measurements. For example, at a $[D_t]$ of 0·4 mM, roughly one-sixth of the dye may be in the dimeric form and at a $[D_t]$ of 1·2 mM, roughly one-third of the dye may be in the dimeric form.

Irrespective of the exact underlying molecular explanation of the effect in Figs. 13 and 14, it is clear that the shapes of the Antipyrylazo III spectra in a 0 mM-Mg^{2+} solution vary with the $[D_t]$. A similar dependence is also seen in Mg^{2+}-containing solutions (not shown). It is important, therefore, when calibrating specific features of dye spectra measured from myoplasm by means of cuvette spectra to evaluate possible effects that are attributable to variations in the $[D_t]$. Two examples relevant to measurements in the text are shown in Fig. 15. Fig. 15*A* shows the values of $\epsilon(550)$, obtained from spectra of the type shown in Fig. 13*A*, as a function of $[D_t]$. Since 550 nm is near an isosbestic point for Mg^{2+} (see below), and $\epsilon(550)$ is near a peak in the absolute absorbance spectrum, the value of $A(550)$ measured from a muscle fibre is useful for estimating the $[D_t]$. Over the range of $[D_t]$ 0–2 mM, which is typical of the muscle experiments, $\epsilon(550)$ varies between 2·8 and $2{\cdot}6 \times 10^{-4}$ M^{-1} cm^{-1}. The most accurate estimates of $[D_t]$ from $A(550)$ would take this variation into account.

However, a value of $2{\cdot}7 \times 10^{-4}$ M^{-1} cm^{-1}, which is within $\pm 4\%$ of the extremes of the range, has been used in most cases when applying eqn. (5) in the text to calculate the $[D_t]$. A quantitatively more important example is shown in Fig. 15*B*, in which cuvette dye absorbances measured at 650 nm, $A(650)$, normalized by those at 550 nm, $A(550)$, are plotted as a function of $[D_t]$. The filled circles are direct measurements from spectra of the type shown in Fig. 13*A* obtained from 0 mM-Mg^{2+} solutions; the dashed curve through these points has been drawn by eye. The continuous curve in Fig. 15*B* (which is appropriate to a free $[Mg^{2+}]$ of 1 mM) was drawn in an analogous fashion, but from data points (not shown) obtained by interpolating between measurements carried out in solutions containing total $[Mg^{2+}]$ of 1 and 2 mM. Interpolation was necessary to obtain this curve, since at the higher $[D_t]$ the dye itself binds significant amounts of Mg^{2+}. (As shown by Rios & Schneider (1981), the binding at lower $[D_t]$ can be described under the assumption of a 1 Mg^{2+}–1 dye complex having a dissociation constant, $K_{D,Mg}$ of 6·7 mM.) Both curves in Fig. 15*B* show an increase in the normalized value $A(650)/A(550)$ as a function of $[D_t]$. The '1 mM' curve (continuous curve), in combination with the muscle isotropic and dichroic spectra of Antipyrylazo III, has been used in the body of the paper (see Table 4) to provide an estimate of the fraction of Antipyrylazo III molecules that are not free in the myoplasmic solution.

Fig. 16 shows examples of the spectral dependence of Antipyrylazo III absorbance on the free $[Mg^{2+}]$ for a low value of $[D_t]$ (0·4 mM, Fig. 16*A*) and a higher value of $[D_t]$ (1·6 mM, Fig. 16*B*). Fig. 16*C* and *D* show the difference spectra, $\Delta A(\lambda)$, respectively, for an increase in free $[Mg^{2+}]$ from 0 to 1·9 mM and from 0 to 1·6 mM. The shapes of the difference spectra are similar (although not identical), revealing a peak decrease in absorbance at 600 nm, smaller positive peaks around 510 and 700 nm, and isosbestic points near 550 and 660 nm. As expected for the smaller change in free $[Mg^{2+}]$, the amplitude of the spectrum in Fig. 16*D* is smaller than that in Fig. 16*C*.

Fig. 17*A* shows the amplitude of $-\Delta A(600)/A(550)$ per unit change in the free $[Mg^{2+}]$ as a function of the $[D_t]$. For the ordinate, the estimates of the change in the free $[Mg^{2+}]$ based on the additions of total Mg^{2+} have been corrected for the binding of Mg^{2+} by the dye. For this purpose, a single $K_{D,Mg}$ of 6·7 mM was assumed to apply, independent of the $[D_t]$. Although this assumption is not likely to be strictly correct, particularly in view of the dimer hypothesis discussed above, it was found to be difficult to study a characterization of the exact dependence experimentally. (The difficulty arose because at the higher values of $[D_t]$ ($> 1{\cdot}6$ mM) and total $[Mg^{2+}]$ (> 2 mM), the dye slowly began to precipitate.) However, since the data in Fig. 17*A* are not strongly dependent on the $[D_t]$, the results indicate that whatever error is introduced by the assumption of a single $K_{D,Mg}$ it may be small for the purposes of calibrating the free $[Mg^{2+}]$, if both the $[Mg^{2+}]$ and the $[D_t]$ are relatively small (< 2–3 mM).

Fig. 17*B* plots the amplitude of the ratio $-\Delta A(720)/\Delta A(600)$ measured from difference spectra of the type shown in Fig. 16*C* and *D*. The amplitude of this parameter increases steeply with the $[D_t]$. This change in shape of the Mg^{2+} difference spectrum with the $[D_t]$ indicates the presence of at least one other dye state besides Mg^{2+}–dye and dye free of Mg^{2+}. Moreover, the increased absorbance at 720 nm with

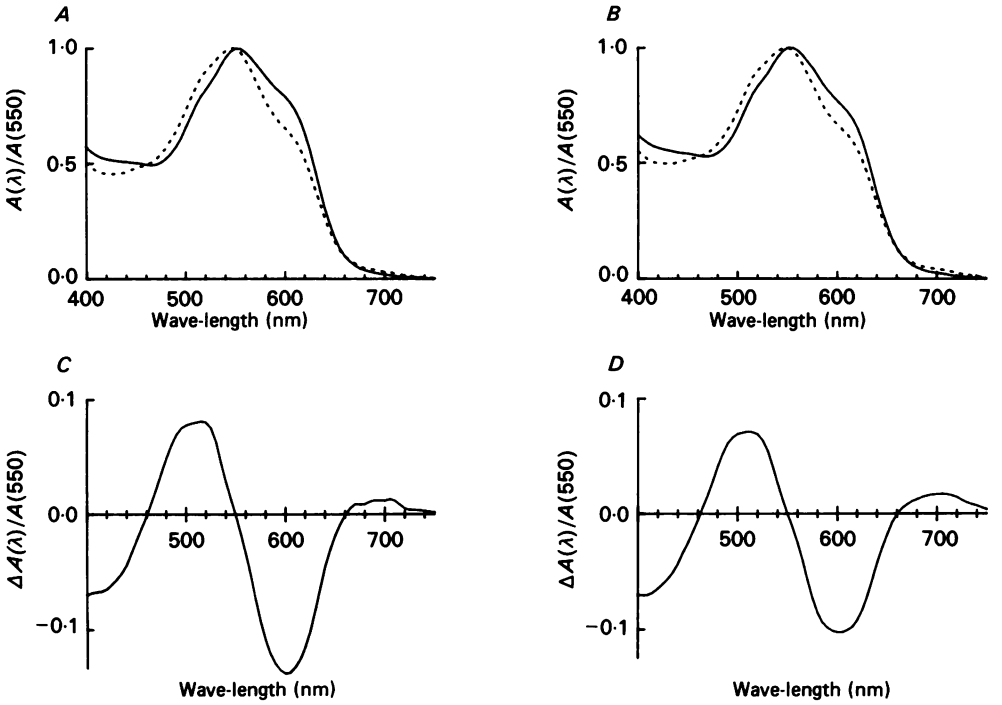

Fig. 16. Calibration spectra for Antipyrylazo III as a function of $[Mg^{2+}]$, obtained at pH 6·90 and a $[D_t]$ of 0·4 mM (*A* and *C*) and 1·6 mM (*B* and *D*). *A*, absolute spectra at a free $[Mg^{2+}]$ of 0 mM (continuous curve) and 1·91 mM (dotted curve) normalized to a value of 1·0 at 550 nm. For the normalization, the scaling factors applied to the two original spectra were identical. *B*, absolute spectra at a free $[Mg^{2+}]$ of 0 mM (continuous curve) and 1·61 mM (dotted curve) normalized to a value of 1·0 at 550 nm. For the normalization, the two scaling factors differed by less than 1 %. *C* and *D*, difference spectra between the absolute spectral pairs in *A* and *B*, respectively.

higher $[D_t]$ (Fig. 17*B*) is in the opposite direction to the (small) contribution to the $\Delta[Mg^{2+}]$ difference spectrum expected from the dissociation of dimers to monomers ($[D_2]$ to $[D]$) in response to the formation of Mg^{2+}–dye (see Fig. 13*B*). The effect could, however, be explained if a one Mg^{2+} to two dye complex that caused an increase in absorbance at long wave-lengths existed, in an analogous manner to the absorbance increase of the one Ca^{2+} to two dye complex (Rios & Schneider, 1981). Whatever the exact explanation, the results point to additional complexity in the chemistry of Antipyrylazo III. In particular, the calibrations indicate that the assumption of a negligible absorbance change at 720 nm from Mg^{2+}–dye complexation, and therefore of non-interference with $\Delta A(720)$ due to Ca^{2+}–dye complexation (Scarpa, Brinley & Dubyak, 1978; Kovacs, Rios & Schneider, 1979, 1983) is not strictly correct. Although the Mg^{2+} effect in Fig. 17*B* is more prominent at higher values of $[D_t]$, it should be noted that if the stoicheiometry of the extra Mg^{2+}–dye complex is one Mg^{2+} to two dye molecules, then the interference with an intracellular $\Delta[Ca^{2+}]$ signal at 720 nm due to a $\Delta[Mg^{2+}]$ signal does not depend on the $[D_t]$. Rather, it depends on

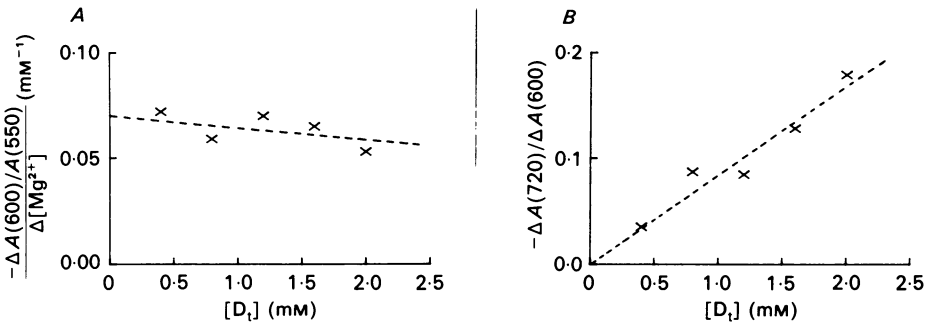

Fig. 17. Selected parameters (crosses) measured from Mg^{2+}–Antipyrylazo III difference spectra (as in Fig. 16*C* and *D*) and plotted as a function of the $[D_t]$. *A*, $\Delta A(600)/A(550)$ per unit change in the free $[Mg^{2+}]$. The dashed line has been fitted by eye. *B*, $-\Delta A(720)/\Delta A(600)$. The dashed line through the origin has been fitted by eye.

the ratio $\Delta[Mg^{2+}]/\Delta[Ca^{2+}]$, since the principal Ca^{2+}–dye stoicheiometry is also 1:2 (Rios & Schneider, 1981).

Finally, the metal-free complexation of Antipyrylazo III described in Figs. 13 and 14 was also looked for in the case of Arsenazo III. A qualitatively similar effect appeared possibly to be present but with a very much smaller amplitude. Therefore, the corresponding effects on the Arsenazo III calibrations have been ignored in the body of the paper.

We thank Dr R. Y. Tsien for the generous gift of a sample of Azo1. We are also grateful to Drs W. K. Chandler, J. G. Maylie and M. F. Schneider for discussions about dye diffusion constants, as well as Dr Chandler and Mr P. Pape for comments on the manuscript. Financial support was provided by the U.S. National Institutes of Health (grants NS–17620 to S.M.B. and NS–15375 to C.S.H.) and the Muscular Dystrophy Association (fellowship to S.H. and grant to C.S.H.).

REFERENCES

BAYLOR, S. M., CHANDLER, W. K. & MARSHALL, M. W. (1979). Arsenazo III signals in singly-dissected frog twitch fibres. *Journal of Physiology* **287**, 23–24*P*.

BAYLOR, S. M., CHANDLER, W. K. & MARSHALL, M. W. (1982*a*). Optical measurement of intracellular pH and magnesium in frog skeletal muscle fibres. *Journal of Physiology* **331**, 105–137.

BAYLOR, S. M., CHANDLER, W. K. & MARSHALL, M. W. (1982*b*). Use of metallochromic dyes to measure changes in myoplasmic calcium during activity in frog skeletal muscle fibres. *Journal of Physiology* **331**, 139–177.

BAYLOR, S. M., CHANDLER, W. K. & MARSHALL, M. W. (1982*c*). Dichroic components of Arsenazo III and Dichlorophosphonazo III signals in skeletal muscle fibres. *Journal of Physiology* **331**, 179–210.

BAYLOR, S. M., CHANDLER, W. K. & MARSHALL, M. W. (1983). Sarcoplasmic reticulum calcium release in frog skeletal muscle fibres estimated from Arsenazo III calcium transients. *Journal of Physiology* **344**, 625–666.

BAYLOR, S. M., CHANDLER, W. K. & MARSHALL, M. W. (1984). Calcium release and sarcoplasmic reticulum membrane potential in frog skeletal muscle fibres. *Journal of Physiology* **348**, 209–238.

BAYLOR, S. M., HOLLINGWORTH, S., HUI, C. S. & QUINTA-FERREIRA, M. E. (1985). Calcium transients from intact frog skeletal muscle fibres simultaneously injected with Antipyrylazo III and Azo1. *Journal of Physiology* **365**, 70*P*.

BAYLOR, S. M. & OETLIKER, H. (1977). A large birefringence signal preceding contraction in single twitch fibres of the frog. *Journal of Physiology* **264**, 141–162.

BAYLOR, S. M., QUINTA-FERREIRA, M. E. & HUI, C. S. (1983). Comparison of isotropic calcium signals from intact frog muscle fibers injected with Arsenazo III or Antipyrylazo III. *Biophysical Journal* **44**, 107–112.

BAYLOR, S. M., QUINTA-FERREIRA, M. E. & HUI, C. S. (1985). Isotropic components of Antipyrylazo III signals from frog skeletal muscle fibers. In *Calcium in Biological Systems*, ed. RUBIN, R. P., WEISS, G. & PUTNEY JR, J. W., pp. 339–349. New York: Plenum Press.

BEELER, T. J., SCHIBECI, A. & MARTONOSI, A. (1980). The binding of Arsenazo III to cell components. *Biochimica et biophysica acta* **629**, 317–327.

BLINKS, J. R., RUDEL, R. & TAYLOR, S. R. (1978). Calcium transients in isolated amphibian skeletal muscle fibres: detection with aequorin. *Journal of Physiology*, **277**, 291–323.

BLINKS, J. R., WIER, W. G., HESS, P. & PRENDERGAST, F. G. (1982). Measurement of Ca^{2+} concentrations in living cells. *Progress in Biophysics and Molecular Biology* **40**, 1–114.

CLOSE, R. I. & LANNERGREN, J. I. (1984). Arsenazo III calcium transients and latency relaxation in frog skeletal muscle fibres at different sarcomere lengths. *Journal of Physiology* **355**, 323–344.

CORAY, A., FRY, C. H., HESS, P., MCGUIGAN, J. A. S. & WEINGART, R. (1980). Resting calcium in sheep cardiac tissue and in frog skeletal muscle measured with ion-selective microelectrodes. *Journal of Physiology* **305**, 60–61*P*.

CRANK, J. (1956). *The Mathematics of Diffusion*. London: Oxford University Press.

GURR, E. (1960). *Encyclopaedia of Microscopic Stains*. Baltimore, MD: Williams & Wilkins.

HAMMING, R. W. (1977). *Digital Filters*. Englewood Cliffs, NJ: Prentice-Hall.

HOLLINGWORTH, S. & BAYLOR, S. M. (1986). Calcium transients in frog skeletal muscle fibers injected with Azo1, a tetracarboxylate Ca^{2+} indicator. In *Optical Methods in Cell Physiology*, ed. DEWEER, P. & SALZBERG, B. M. New York: Wiley and Sons.

IRVING, M., CHANDLER, W. K., MAYLIE, J. & SIZTO, N. L. (1985). Antipyrylazo III calcium transients in cut frog twitch fibers. *Biophysical Journal* **47**, 350a.

KOVACS, L., RIOS, E. & SCHNEIDER, M. F. (1979). Calcium transients and intramembrane charge movement in skeletal muscle fibres. *Nature* **279**, 391–396.

KOVACS, L., RIOS, E. & SCHNEIDER, M. F. (1983). Measurement and modification of free calcium transients in frog skeletal muscle fibres by a metallochromic indicator dye. *Journal of Physiology* **343**, 161–196.

KOVACS, L., SCHUMPERLI, R. A. & SZUCS, G. (1983). Comparison of birefringence signals and calcium transients in voltage clamped cut skeletal muscle fibres of the frog. *Journal of Physiology* **341**, 579–593.

KOVACS, L. & SZUCS, G. (1983). Effect of caffeine on intramembrane charge movement and calcium transients in cut skeletal muscle fibres of the frog. *Journal of Physiology* **341**, 559–578.

KUSHMERICK, M. J. & PODOLSKY, R. J. (1969). Ionic mobility in muscle cells. *Science* **166**, 1297–1298.

LOPEZ, J. R., ALAMO, L., CAPUTO, C., DIPOLO, R. & VERGARA, J. (1983). Determination of ionic calcium in frog skeletal muscle fibers. *Biophysical Journal* **43**, 1–4.

MAYLIE, J., CHANDLER, W. K., IRVING, M. & SIZTO, N. L. (1985). Late Antipyrylazo III signals in cut muscle fibers. *Biophysical Journal* **47**, 351a.

MELZER, W., RIOS, E. & SCHNEIDER, M. F. (1984). Time course of calcium release and removal in skeletal muscle fibers. *Biophysical Journal* **45**, 637–641.

MELZER, W., RIOS, E. & SCHNEIDER, M. F. (1986). The removal of myoplasmic free calcium following calcium release in frog skeletal muscle. *Journal of Physiology* **372**, 261–292.

MILEDI, R., PARKER, J. & SCHALOW, G. (1977). Measurement of calcium transients in frog muscle by the use of Arsenazo III. *Proceedings of the Royal Society* B **198**, 201–210.

MILEDI, R., PARKER, I. & SCHALOW, G. (1979). Transition temperature of excitation–contraction coupling in frog twitch muscle fibres. *Nature* **280**, 326–328.

MILEDI, R., PARKER, I. & ZHU, P. H. (1982). Calcium transients evoked by action potentials in frog twitch muscle fibres. *Journal of Physiology* **333**, 655–679.

MILEDI, R., PARKER, I. & ZHU, P. H. (1983*a*). Calcium transients in frog skeletal muscle fibres following conditioning stimuli. *Journal of Physiology* **339**, 223–242.

MILEDI, R., PARKER, I. & ZHU, P. H. (1983*b*). Calcium transients studied under voltage-clamp control in frog twitch muscle fibres. *Journal of Physiology* **340**, 649–680.

OCHI, K. & MATSUMURA, M. (1984). Arsenazo III signals following action potential as influenced by nitrate in *Xenopus* skeletal muscle. *Japanese Journal of Physiology* **34**, 361–364.

PALADE, P. & VERGARA, J. (1981). Detection of Ca^{++} with optical methods. In *Regulation of Muscle Contraction: Excitation–Contraction Coupling*, ed. GRINNELL, A. D., & BRAZIER, MARY A. B., pp. 143–160. New York: Academic Press.

PALADE, P. & VERGARA, J. (1982). Arsenazo III and antipyrylazo III calcium transients in single skeletal muscle fibers. *Journal of General Physiology* **79**, 679–707.

QUINTA-FERREIRA, M. E., BAYLOR, S. M. & HUI, C. S. (1984*a*). Antipyrylazo III (Ap III) and Arsenazo III (Az III) calcium transients from frog skeletal muscle fibers simultaneously injected with both dyes. *Biophysical Journal* **45**, 47a.

QUINTA-FERREIRA, M. E., BAYLOR, S. M. & HUI, C. S. (1984*b*). Myoplasmic Ca transients and sarcoplasmic reticulum Ca movements in frog skeletal muscle fibers injected with Antipyrylazo III. *Proceedings of the International Union for Pure and Applied Biophysics* (Bristol, England), p. 207.

RIOS, E. & SCHNEIDER, M. F. (1981). Stoichiometry of the reactions of calcium with the metallochromic indicator dyes Antipyrylazo III and Arsenazo III. *Biophysical Journal* **36**, 607–621.

RIOS, E., STEFANI, E., BRUM, G. & GOLDMAN, J. (1985). Extracellular Ca modifies Ca release from the sarcoplasmic reticulum (SR) in skeletal muscle fibers. *Biophysical Journal* **47**, 353a.

SCARPA, A., BRINLEY, F. J. & DUBYAK, G. (1978). Antipyrylazo III, a 'middle range' Ca^{2+} metallochromic indicator. *Biochemistry* **17**, 1378–1386.

SCHNEIDER, M. F., RIOS, E. & KOVACS, L. (1981). Calcium transients and intramembrane charge movement in skeletal muscle. In *Regulation of Muscle Contraction: Excitation–Contraction Coupling*, ed. GRINNELL, A. D. & BRAZIER, MARY A. B., pp. 131–141. New York: Academic Press.

STRETTON, A. O. W. & KRAVITZ, E. A. (1973). Intracellular dye injection: the selection of Procion Yellow and its application in preliminary studies of neuronal geometry in the lobster nervous system. In *Intracellular Staining in Neurobiology*, ed. KATER, S. B. & NICHOLSON, C., pp. 21–40. New York: Springer-Verlag.

TSIEN, R. Y. (1980). New calcium indicators and buffers with high selectivity against magnesium and protons: design, synthesis, and properties of prototype structures. *Biochemistry* **19**, 2396–2404.

TSIEN, R. Y. (1983). Intracellular measurements of ion activities. *Annual Review of Biophysics and Bioengineering* **12**, 91–116.